



Paleomagnetism of Mesoproterozoic margins of the Anabar Shield: A hypothesized billion-year partnership of Siberia and northern Laurentia

David A.D. Evans^{a,*}, Roman V. Veselovsky^{b,c}, Peter Yu. Petrov^d, Andrey V. Shatsillo^b, Vladimir E. Pavlov^{b,e}

^a Department of Geology & Geophysics, Yale University, New Haven, USA

^b Institute of Physics of the Earth, Russian Academy of Science, Moscow, Russia

^c Geological Department, Lomonosov Moscow State University, Moscow, Russia

^d Geological Institute, Russian Academy of Science, Moscow, Russia

^e Kazan Federal University, Kazan, Russia

ARTICLE INFO

Article history:

Received 5 February 2016

Revised 23 May 2016

Accepted 12 June 2016

Available online 17 June 2016

Keywords:

Siberia

Anabar

Riphean

Paleomagnetism

Nuna

Rodinia

ABSTRACT

Siberia and Laurentia have been suggested as near neighbors in Proterozoic supercontinents Nuna and Rodinia, but paleomagnetic evidence has been sparse and ambiguous. Here we present four new paleomagnetic poles from undeformed Paleo-Mesoproterozoic (lower Riphean) sedimentary rocks and mafic intrusions of the northwestern Anabar uplift in northern Siberia. Combining these results with other Proterozoic data from Siberia and Laurentia, we propose a tight juxtaposition of those two blocks (Euler parameters 77°, 098°, 137° for Anabar to North America) spanning the interval 1.7–0.7 Ga, constituting a long-lived connection that outlasted both the Nuna and Rodinia supercontinental assemblages.

© 2016 Elsevier B.V. All rights reserved.

1. Introduction

Proterozoic continental reconstructions are crucial for understanding long-term Earth history, but their development has occurred over decades with some major components yet unresolved, including precise configurations of the supercontinents Nuna and Rodinia (reviewed by Evans, 2013). Paleomagnetic data are an integral component of such reconstructions, but the Proterozoic database has been dominated by results from Laurentia and Baltica (Buchan, 2013). The present study addresses reconstruction of Siberia, one of the major Proterozoic cratons. Siberia's paleogeographic relationship to Laurentia has been contentious, with juxtapositions ranging from Laurentia's western margin (Sears and Price, 1978, 2000, 2003) to its northern margin in a variety of orientations (Hoffman, 1991; Condie and Rosen, 1994; Frost et al., 1998; Rainbird et al., 1998).

In the past 15 years, paleomagnetic data have strongly supported a mid-Proterozoic location of Siberia near Laurentia's northern margin, such that southern Siberia faced northern Laurentia (Gallet et al., 2000; Ernst et al., 2000; Pavlov et al., 2002; Metelkin et al., 2007; Wingate et al., 2009; Didenko et al., 2009). An unresolved issue is whether such a fit is loose, in which the

two cratons were separated by several thousand km (Pisarevsky and Natapov, 2003; Pisarevsky et al., 2008) or tight (Pavlov et al., 2002; Metelkin et al., 2007; Evans and Mitchell, 2011). The loose-fit hypothesis is inspired primarily due to a perceived incongruity between 1.1 and 1.0 Ga poles from the two cratons, but as will be described further, such a conclusion rests on ages of Siberian sedimentary strata with rather poor constraints. Evans and Mitchell (2011) proposed the two cratons to be tightly joined in Nuna but separating through the interval 1.38–1.27 Ga—the era of numerous mafic intrusive events throughout Laurentia, Siberia, and neighboring Baltica—to achieve the more distant relative position apparently required by the 1.1–1.0 Ga poles. Nonetheless, the matching LIP “barcode” record spanning 1.7–0.7 Ga from Laurentia and Siberia (Gladkochub et al., 2010a; Ernst et al., 2016a) may alternatively suggest a tight fit between the two blocks enduring as late as 0.7 Ga. A relative lull in tectonic activity or sedimentary record (e.g. passive margins) in southern Siberia throughout that interval could also suggest that margin's location within a continental interior (Gladkochub et al., 2010b). It is more difficult to apply the same test to northern Laurentia, because that margin is largely covered by Phanerozoic strata (e.g., Kerr, 1982).

The purpose of this paper is to report new paleomagnetic data from nearly pristine igneous and sedimentary rocks of the Anabar uplift in northern Siberia, to assess the aggregate paleomagnetic

* Corresponding author.

record of Siberia and Laurentia in Proterozoic time, and to propose a new, static configuration between the two blocks that honors both the geologic and paleomagnetic datasets. Preliminary data from some of the sites described herein were reported by Veselovskiy et al. (2009), but our present contribution supersedes the western and northern Anabar datasets reported in that earlier paper.

2. Geologic setting

The Siberian craton, which assembled at about 1900 Ma (Rosen, 2003), is largely covered by Phanerozoic sedimentary rocks. Precambrian rocks, both crystalline and sedimentary, are exposed around the craton's margins as well as two shield areas or uplifts: Anabar in the northwest, and Aldan in the southeast (Fig. 1). Both shield areas (i.e., exposed crystalline basement) are mantled by sedimentary cover and inferred to represent larger, internally coherent blocks. Whereas the Aldan block exposes much of its pre-Phanerozoic basement architecture, the Anabar block is almost entirely covered. In the north-central Anabar block, a gentle domal uplift exposes the Anabar Shield and an annular ring of Mesoproterozoic (Riphean) sedimentary rocks that are invaded by numerous mafic intrusions. Geophysical surveys (e.g., Rosen et al., 1994) extend the inferred basement architecture of the Anabar block beyond its uplifted shield regions, under its sedimentary cover (also described by Pisarevsky et al., 2008). There is increas-

ingly compelling paleomagnetic evidence for a 20–25° relative rotation between the Anabar and Aldan blocks during Devonian formation of the Vilyuy rift system (Pavlov and Petrov, 1997; Smethurst et al., 1998; Gallet et al., 2000; Pavlov et al., 2008). Aside from this deformation, the Siberian cratonic interior has remained tectonically stable other than emplacement of Devonian–Triassic kimberlites and the particularly voluminous Permian–Triassic “traps” (largely mafic, both extrusive and intrusive; Nikishin et al., 2010).

The Anabar uplift, which is the study area of this work, is a broad cratonic arch with Paleoproterozoic crystalline basement (shield) encircled by nonconformably overlying, nearly horizontal and regionally unmetamorphosed, Paleo-Mesoproterozoic sedimentary rocks (Fig. 1). The sedimentary succession begins with clastic strata of the Mukun Group, transitioning upsection to carbonates of the Billyakh Group (Figs. 1 and 2). The lowest clastic layers contain detrital zircons as young as 1681 ± 28 Ma ($n = 8$; Khudoley et al., 2015), providing a maximum constraint for the onset of sedimentation. Mafic sills intrude the stratigraphy at several levels, and there are numerous mafic dykes as well. The most common ages for dated intrusions are ca. 1500–1470 Ma (reviewed by Gladkochub et al., 2010a; new data presented in Ernst et al., 2016b), the latter figure being shared by mafic magmatism in the Olenëk uplift about 600 km to the east (Wingate et al., 2009); but many Anabar intrusions are suspected to be related to the Permian–Triassic traps (Bogdanov et al., 1998).

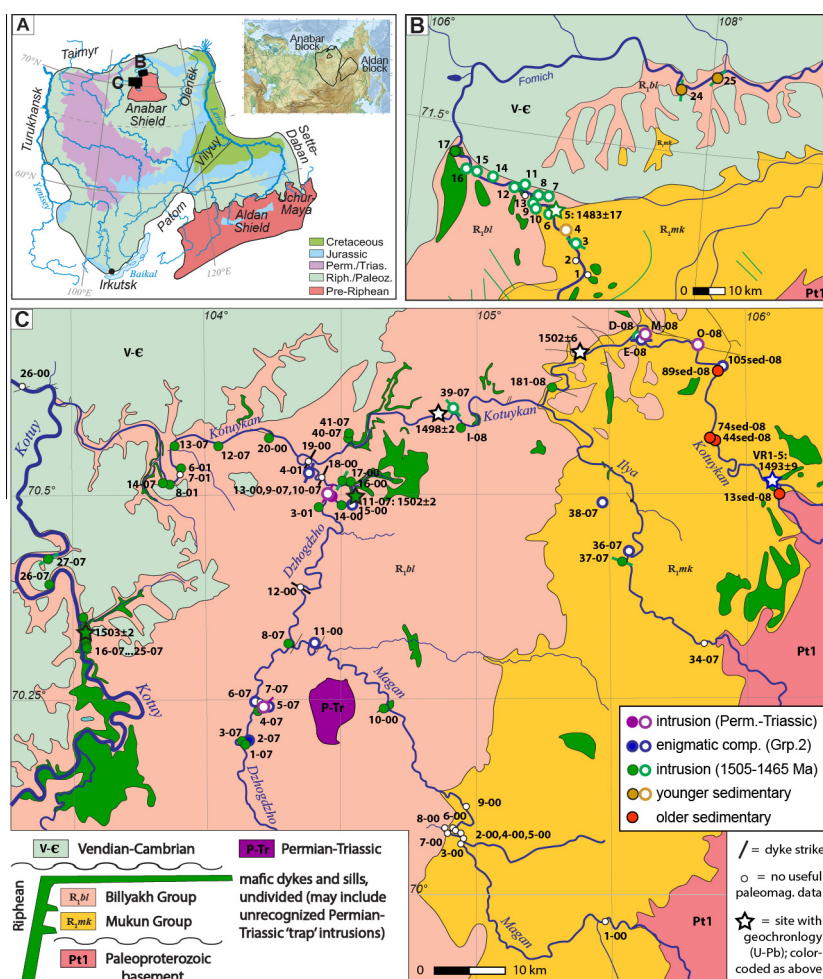


Fig. 1. Regional map of Siberian craton (A), highlighting the location of Anabar Shield study areas (B, C). Paleomagnetic sampling sites are color-coded according to characteristic remanent magnetization (ChRM) group. Filled = normal polarity, open = reversed polarity.

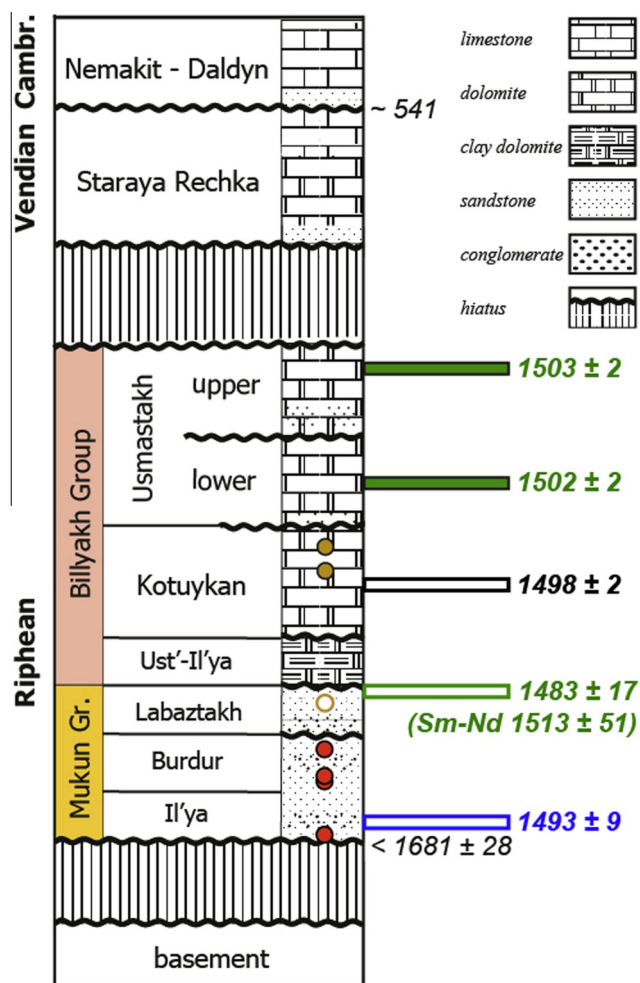


Fig. 2. Schematic stratigraphic column (not to scale) for the northwestern flank of the Anabar Shield. Vertical lines represent unconformities. Circles represent sedimentary paleomagnetic sampling horizons. These, and approximate mafic sill levels (with U–Pb ages from Ernst et al., 2016b), are color-coded for ChRM group and polarity interpretation as in Fig. 1. Other ages are discussed in the text.

3. Methods

In this study, paleomagnetic samples were collected from both the lower clastic and upper carbonate stratigraphic units of the Riphean succession, and from numerous mafic intrusions, some of them directly dated by U–Pb ages on baddeleyite (Ernst et al., 2016b). We report data from six raft trips in the northern flank (Fomich River) and western flank (Kotuy, Dzhogdzh, Magan, Ilya, and Kotuykan Rivers) of the Anabar dome, where strata everywhere dip less than 5°. The sites were mainly block-sampled, except for portable-drilled samples on the upper reaches of the Kotuykan River. Orientation was achieved by magnetic compass and clinometer, occasionally supplemented by solar compass and indicating local magnetic variations that match expected IGRF values to within a few degrees. Representative samples from a subset of the sites were investigated by optical and scanning-electron microscopy.

Demagnetization was performed within shielded chambers in the following paleomagnetic laboratories: Institute of Physics of the Earth (Moscow), Institut de Physique du Globe (Paris) and Yale University (New Haven). Following measurement of the natural remanent magnetization (NRM), all samples were thermally demagnetized up to 580–680 °C with an average of 12–15 steps to isolate the components of the natural remanent magnetization.

The measurements were made using a 2G-Enterprise cryogenic magnetometer (Paris, Yale), and an AGICO JR-6 spinner magnetometer (Moscow); heating was done in homemade non-magnetic ovens (Paris), a MMTD-80 (Magnetic Measurements Ltd.) thermal demagnetizer (Moscow), and a TD-48 (ASC Scientific) thermal demagnetizer (Yale). Some specimens were pre-treated by low-temperature immersion in liquid nitrogen to remove multi-domain magnetic components (Borradaile et al., 2004), but we found that such procedure had little effect on the quality of data acquired during the subsequent high-temperature demagnetization. Directional data were fit in almost all cases with least-squares lines, but occasionally least-squares planes or great circles, according to routines developed by Kirschvink (1980) and Enkin (1994). Reconstructions were made using the GPlates freeware package (Williams et al., 2012).

4. Results

About half of the samples yielded well resolved components of the NRM (Table 1). Most of those samples contained only one or two components (Figs. 3–6), with one clearly defined characteristic remanence magnetization (ChRM). Within the sedimentary rocks distant to mapped intrusions, which were red-colored, unblocking temperatures extend as high as ~680 °C, indicating near-stoichiometric hematite as the remanence carrier (Fig. 3). Within mafic rocks, unblocking temperatures extend as high as ~580 °C, indicating low-Ti titanomagnetite as the carrier (Figs. 4–6). Some mafic specimens display two components of magnetization that are nearly antipodal, (e.g., Fomich site 17, Dzhogdzh trap sites 9-07 and 13-00) indicating either intrinsic self-reversal behavior (e.g., Krása et al., 2005; Gapeev and Gribov, 2008), remanence acquisition over a protracted interval of time spanning a geomagnetic field reversal, or a spurious artifact associated with stepwise heating (Shcherbakov et al., 2015).

Site-mean directions are listed in Table 1. We applied data quality filters on the number of least-squares lines and/or circles (the latter counting half, total per site >4) and Fisher's (1953) 95% confidence radius ($\alpha_{95} < 20^\circ$). Characteristic remanence directions vary according to lithology (Fig. 7). Sedimentary rocks that are distant (i.e., more than a few hectometers) to mapped intrusions, in general, yield either S-down or N-up ChRMs. There is a systematic shift in declination between the lower sedimentary horizons and the upper units, but the directional shift does not occur along the boundary between the Mukun and Billyakh Groups. Instead, the shift is localized between the Burdur and Labaztakh Formations, within the upper part of the Mukun Group, where a disconformity is recognized regionally (Fig. 2). The “older sedimentary” directional group contains only one polarity, whereas the “younger sedimentary” group contains two polarities.

Within intrusive units, ChRMs fall into four distinct groups: (1) a steep, two-polarity group with W-up and E-down directions, (2) a moderate-inclination component with mainly N-down directions but a single site of opposite S-up polarity, (3) a shallow NE direction, mainly downward, from the Fomich River, and (4) a shallow SW direction, upward, from the western Anabar region plus the stratigraphically uppermost site of Fomich River. Group 1 likely represents intrusions from the Permian–Triassic Siberian trap large igneous province, based on similarity of directions to published results (Pavlov et al., 2011). Group 2 is termed the “enigmatic” component, and will be discussed at length, below. Groups 3 and 4 are broadly antipodal, but a formal significance test (McFadden and McElhinny, 1990) reveals that antiparallelism can be rejected at the 95% confidence level (i.e., the two groups “fail” the reversal test by standard measure; although they are within antiparallelism at slightly more lax 99% confidence limits). Some of the departure

Table 1
Paleomagnetic data from the northern and western margins of the Anabar Shield, Siberia.

Site abbr.	River section	Lithology	Weight	Lat.(°N)	Long.(°E)	n/N	GDec	GInc	k	a95	Plat(N)	Plong(E)	U–Pb geochronology or geochemistry
<i>Older sediments</i>													
1-04	Fomich	Burdur Fm., pink sandstone	0(PLF)	71.2067	107.2928	10/15	359.3	75.1	45.7	7.2	–	–	
2-04	Fomich	Burdur Fm., pink-cherry sandstone	0(PLF)	71.2425	107.1817	15/15	351.8	78.0	43.0	5.9	–	–	
3-04(H)	Fomich	Upper Burdur Fm., distant host rocks to 04-3(D)	0(scatter)	71.2767	107.1442	0/10	Unstable	–	–	–	–	–	
13sed-08	Upper Kotuykan	Il'ya Fm., red sandstone	1	70.5016	106.1270	12/31	165.7	30.9	19.8	10.0	–02.3	119.8	
44sed-08	Upper Kotuykan	Burdur Fm., chocolate, cherry-colored ss.	1	70.563	105.883	20/30	156.1	30.0	10.1	10.8	–01.8	128.8	
74sed-08	Upper Kotuykan	Burdur Fm., red sandstone	1	70.5697	105.8727	6/15	173.5	30.1	28.4	12.8	–03.1	112.1	
89sed-08	Upper Kotuykan	Burdur Fm., red sandstone	1	70.6468	105.9104	10/16	167.1	19.2	9.4	16.6	–09.0	118.8	
34-07	Ilya	Il'ya Fm., red sandstone	0(scatter)	70.3138	105.8413	0/13	Unstable	–	–	–	–	–	
1-00	Magan	Burdur Fm., sandstone	0(scatter)	69.97	105.47	0/67	Unstable	–	–	–	–	–	
<i>Mean</i>						4 sites	165.6	27.7	92.9	9.6	–04.1	119.9	K = 113 A95 = 8.7
<i>Younger sediments</i>													
4-04	Fomich	Labaztakh Fm., cherry-colored siltstone	1	71.3194	107.0375	20/20	016.7	–28.0	80.0	3.7	–3.0°	90.9°	
24-04(H)	Fomich	Kotuykan Fm., gray limestone 100–350 m away from dyke at 04-24(D)	1	71.6403	107.7739	7/31	194.4	35.2	21.3	13.4	01.6	094.2	
25-04(H)	Fomich	Kotuykan Fm., variegated limestone 150 m away from dyke at 04-25(D)	1	71.6708	108.0250	11/22	193.0	33.5	12.5	13.4	00.4	095.7	
7-07	Dzhogdzho	Kotuykan Fm., red dolostone	0(scatter)	70.234	104.172	0/11	Scattered	–	–	–	–	–	
2-00	Magan	Labaztakh Fm., red sandstone	0(scatter)	70.07	104.92	0/20	Unstable	–	–	–	–	–	
3-00	Magan	Labaztakh Fm., sandstone	0(scatter)	70.05	104.95	0/7	Unstable	–	–	–	–	–	
4-00	Magan	Labaztakh Fm., sandstone	0(scatter)	70.07	104.92	0/16	Unstable	–	–	–	–	–	
5-00	Magan	Labaztakh and Ust-Il'ya Fms., sandstone	0(scatter)	70.07	104.92	0/12	Unstable	–	–	–	–	–	
6-00	Magan	Ust-Il'ya Fm.	0(scatter)	70.07	104.90	0/10	Unstable	–	–	–	–	–	
7-00	Magan	Ust-Il'ya Fm.	0(scatter)	70.07	104.88	0/14	Unstable	–	–	–	–	–	
8-00	Magan	Ust-Il'ya Fm., sandstone	0(scatter)	70.07	104.88	0/16	Unstable	–	–	–	–	–	
9-00	Magan	Lowest part of Ust-Il'ya Fm., sandstone	0(scatter)	70.07	104.93	0/17	Unstable	–	–	–	–	–	
<i>Mean</i>						3 sites	194.7	32.2	393.0	6.2	–00.3	093.6	K = 553 A95 = 5.2
<i>Steep W-up/E-down "Permian-Triassic" (Group 1)</i>													
0-08(D)	Upper Kotuykan	Dolerite sill	0.5	70.6880	105.8291	8/12	271.5	–68.9	214.1	3.8	47.9°	171.4°	
0-08(C,H)	Upper Kotuykan	Exocontact and host rocks to 0-08(D)	0.5	70.6880	105.8291	21/23	276.4	–72.5	136.6	2.7	51.1°	163.5°	
M-08	Upper Kotuykan	Mafic sill	1	70.7022	105.6473	13/15	257.8	–76.4	64.6	5.2	61.6°	169.3°	
5-07(D)	Dzhogdzho	3–4 m wide mafic dyke, trending 045°	0.5	70.2331	104.1851	6/10	010.9	–77.3	82.0	7.4	46.2°	97.7°	
5-07(C)	Dzhogdzho	Exocontact to 5-07(D)	0.5	70.2331	104.1851	4/10	359.5	–70.4	47.5	13.5	34.8°	104.5°	
7-07	Dzhogdzho	Kotuykan Fm., red dolostone (remagnetized by nearby, unmapped P-Tr intrusion?)	1	70.234	104.172	9/10	079.7	70.5	19.6	11.9	53.4	176.7	
13-00	Dzhogdzho	Mafic dyke, trending 030°	1	70.5025	104.4367	9/15	071.2	81.0	26.5	10.2	68.6	156.1	
9-07	Dzhogdzho	Weathered mafic dyke, 15 m wide, trending 030°	1	70.5028	104.4396	17/21	118.3	79.8	51.7	5.0	56.4	137.1	
10-07	Dzhogdzho	Mafic sill, 4 m thick	1	70.5028	104.4396	6/12	222.2	–71.3	168.6	5.2	66.8°	211.4°	

Mean							7 sites	089.3	78.4	48.9	8.7	61.0 K = 15.1	155.6 A95 = 16.1	
N-down/S-up “enigmatic component” (Group 2)														
VR1-08	Upper Kotuykan	Large (>10 m thick), fresh mafic sill at river level	0.2	70.5155	106.1041	8/8	023.0	67.7	65.0	6.9	67.5	245.8		
VR2-08	Upper Kotuykan	Same sill as VR1, sampled ~3 m higher	0.2	70.515	106.102	8/8	032.8	67.3	98.3	5.6	64.6	232.1		
VR3-08	Upper Kotuykan	Same sill as VR2, sampled ~2 m higher	0.2	70.515	106.101	8/8	044.2	63.8	41.8	8.7	57.1	221.9		
VR4-08	Upper Kotuykan	Same sill as VR3, sampled ~2 m higher	0.2	70.515	106.099	7/8	013.9	64.7	46.6	8.9	65.2	263.0	1493 ± 6 Ma (same sill, 400 m away)	
VR5-08	Upper Kotuykan	Same sill as VR4, at its fine-grained margin	0.2	70.5192	106.0625	8/8	028.7	65.8	91.5	5.8	63.7	239.6	1493 ± 6 Ma (same sill, 1100 m away)	
105sed-08	Upper Kotuykan	Ilya and Burdur Formations, redbeds	1	70.653	105.932	10/12	028.5	42.8	124.3	4.3	41.3	250.7		
E-08	Upper Kotuykan	Mafic sill or dyke, trending E-W, crossing river valley	1	70.697	105.642	14/15	026.7	53.3	35.7	6.7	50.4	249.8		
36-07	Ilya	Coarse, dark green mafic body, 50 m of exposure	1	70.4240	105.5732	10/15	022.2	60.0	91.2	5.1	58.4	252.6		
38-07	Ilya	Mafic sill(?) at least 18 m thick	1	70.4851	105.4752	9/10	008.6	52.0	41.7	8.1	51.8	273.7		
11-00	Magan	Mafic sill, mapped as P-Tr	1	70.3111	104.4033	11/11	356.9	57.7	108.4	4.4	58.0	289.0		
2-07	Dzhogdzho	Fine, green-black gabbro-dolerite sill >15 m thick	1	70.1953	104.1407	13/16	186.5	−54.2	20.4	9.4	54.4	275.0		
5-07(H)	Dzhogdzho	Kotuykan Fm., red dolostone host to 5-07(D)	1	70.2331	104.1851	3/28	352.6	60.0	10.6	16.6	60.4	295.6		
6-07	Dzhogdzho	Kotuykan Fm., red dolostone	1	70.2346	104.1749	9/9	329.2	58.3	35.4	11.4	54.9	327.9		
15-00	Dzhogdzho	Same large mafic sill as 11-07 and 16-00 (Group 4)	1	70.4878	104.5219	5/15	037.7	56.2	46.7	11.3	50.9	233.6		
18-00	Dzhogdzho	Weathered dyke, trending 025°	0(scat)	70.5228	104.4242	0/15	Unstable	−	−	−	−	−		
4-01	Dzhogdzho	Mafic dyke <1 m wide, trending 025°	1	70.53	104.37	8/8	316.4	70.1	68.0	6.8	64.9	356.5		
19-00	Dzhogdzho	Mafic dyke, trending 030°	0(scat)	70.5417	104.3683	0/15	Unstable	−	−	−	−	−		
Mean							11 sites	009.6	59.4	30.7	8.4	60.1 K = 15.8	271.9 A95 = 11.8	
NE-shallow (Group 3)														
3-04(D)	Fomich	50 m wide dolerite dyke, trending 300°	0.5	71.2767	107.1442	14/15	032.3	−05.0	59.7	5.2	13.3	253.9		
3-04(C)	Fomich	Contact rocks to 04-3(D), upper Burdur Fm.	0.5	71.2767	107.1442	9/15	034.2	−03.2	56.0	6.9	13.8	251.8		
5-04	Fomich	Dolerite sill	0.5	71.3422	106.9244	10/15	024.5	22.6	16.9	12.1	28.6	259.4	Geochemistry group I; 1483 ± 17 Ma	
6-04	Fomich	Dolerite sill (same as 04-6)	0.5	71.3408	106.9278	14/14	024.3	17.9	16.2	10.2	26.0	260.0		
7-04	Fomich	Dolerite sill	0.25	71.3772	106.8511	13/15	024.1	07.0	26.5	8.2	20.4	261.1		
8-04	Fomich	Dolerite sill (same as 04-7)	0.25	71.3786	106.8400	14/15	020.9	16.7	16.5	10.1	25.8	263.8		
9-04	Fomich	Dolerite sill (same as 04-7)	0.25	71.3636	106.8056	15/15	020.6	04.0	23.6	8.0	19.4	264.9	Geochemistry group I	
10-04	Fomich	Dolerite sill (same as 04-7)	0.25	71.3658	106.8142	9/15	009.1	16.5	14.6	13.9	26.8	276.7		
11-04	Fomich	Dolerite sill	0.5	71.3747	106.7314	10/15	015.8	09.0	21.0	10.8	22.4	269.7		
12-04	Fomich	Dolerite sill (same as 04-11)	0.5	71.3717	106.7281	10/10	024.1	−01.2	83.1	5.3	16.4	261.5		
13-04	Fomich	Dolerite sill (same as 04-12)	0(scat)	71.3722	106.7161	9/10	001.7	−06.3	7.0	20.9	15.5	285.0		
14-04	Fomich	Dolerite	1	71.3928	106.5356	7/11	023.3	12.6	27.1	11.8	23.4	261.2		
15/16-04	Fomich	Dolerite sill	1	71.409	106.380	9/22	039.3	07.2	9.4	17.7	17.8	244.8	Geochemistry group II	
24-04(D)	Fomich	30 m wide dolerite dyke, trending 005°	0(scat)	71.6403	107.7739	7/15	024.6	−08.6	11.5	18.6	12.4	262.6	Geochemistry group II	
D-08	Upper Kotuykan	Gabbro-dolerite sill	1	70.7005	105.6013	11/11	039.7	09.1	13.4	12.9	19.2	243.2		
39-07(D)	Upper Kotuykan	20 m wide dolerite dyke, trending 320°	1	70.6059	104.9124	14/14	035.7	34.8	27.9	7.7	34.4	243.0		
39-07(C)	Upper Kotuykan	Baked contact rocks to 39-07(D)	0(scat)	70.6059	104.9124	4/12	010.8	56.3	16.8	23.1	55.8	269.5		
39-07(H)	Upper Kotuykan	Host rocks to 39-07(D), Kotuykan Fm.	1	70.6059	104.9124	6/9	020.0	30.6	29.7	12.5	34.5	261.5		

(continued on next page)

Table 1 (continued)

Site abbr.	River section	Lithology	Weight	Lat.(°N)	Long.(°E)	n/N	GDec	GInc	k	a95	Plat(N)	Plong(E)	U–Pb geochronology or geochemistry
<i>Mean</i>						9 sites	028.3	14.1	27.4	10.0	23.9 K = 48.0	255.3 A95 = 7.5	
<i>SW-shallow (Group 4)</i>													
17-04	Fomich	Dolerite sill (Tunbl > 500 °C)	1	71.4317	106.2567	7/11	217.6	–35.0	58.4	8.0	–33.5	062.6	
25-04(D)	Fomich	10 m wide dolerite dyke, trending 045°	0(scatter)	71.6708	108.0250	(4 + 2c)/10	225.0	19.8	11.9	21.0	–02.9	063.8	
25-04(C)	Fomich	Exocontact to 25–04(D); green limestone	0 (anom)	71.6708	108.0250	9/9	251.6	06.1	195.5	3.7	–02.8	036.5	
181-08(DC)	Upper Kotuykan	Dolerite dyke (trending NNW) and baked contact rocks	1	70.6333	105.2690	12/32	206.9	–11.6	24.3	9.0	–23.0	076.0	
1-08	Upper Kotuykan	5 m wide dolerite dyke	1	70.5895	104.9653	11/12	215.7	–19.7	77.3	5.2	–25.6	065.4	
40-07	Upper Kotuykan	Dolerite sill, at least 18 m thick	0.5	70.5670	104.5259	14/16	223.9	–24.2	80.2	4.5	–26.1	055.6	
41-07	Upper Kotuykan	Dolerite sill, same as 40–07	0.5	70.5634	104.5381	10/12	223.1	–27.6	26.1	9.6	–28.3	055.9	
37-07(D)	Ilya	12 m wide dolerite dyke, trending 290°	1	70.4206	105.5630	11/12	232.8	–17.1	36.4	7.7	–20.1	048.6	
37-07(C)	Ilya	Baked contact rocks to 37–07(D)	0(scatter)	70.4206	105.5630	4/7	231.4	–21.8	25.0	18.7	–22.9	049.2	
37-07(H)	Ilya	Host rocks to 37–07(D), lower Burdur Fm.	0(few)	70.4206	105.5630	(1 + 3c)/9	230.5	–25.6	194.3	9.0	–25.3	049.5	
10-00	Magan	Mafic intrusion	1	70.2358	104.6681	7/15	227.8	–18.8	17.0	15.1	–22.4	052.5	
1-07	Dzhogdzho	Dolerite sill, at least 10 m thick	1	70.1847	104.1219	13/15	214.1	–22.3	51.6	5.8	–27.6	065.8	
3-07	Dzhogdzho	Dolerite sill with differentiated center	1	70.1929	104.1194	16/24	224.0	–20.3	44.8	5.6	–24.3	055.6	ca.1770 Ma, zircon (xenocr.)
4-07	Dzhogdzho	Fine-grained mafic sill	1	70.2281	104.1778	17/27	211.7	–17.8	32.3	6.4	–25.7	069.0	
12-00	Dzhogdzho	Mafic dyke, trending 300°	0(scatter)	70.3869	104.3358	0/12	Unstable	–	–	–	–	–	
8-07	Dzhogdzho	Mafic intrusion	0(few)	70.3094	104.3128	(3 + 2c)/15	212.1	–18.2	52.3	11.4	–25.7	068.7	
3-01	Dzhogdzho	Dolerite sill	1	70.47	104.45	13/15	219.0	–33.9	44.8	6.3	–33.1	059.0	
14-00	Dzhogdzho	Dolerite sill, maybe same as 11–07 and 16–00?	1	70.4878	104.4889	5/16	222.5	–20.2	108.7	7.4	–24.4	057.6	
11-07(S)	Dzhogdzho	Dolerite sill, same as 16–00	0.333	70.4964	104.5335	9/10	246.3	–30.4	79.7	5.8	–23.2	031.6	Transitional geochemistry; 1502 ± 2 Ma
11-07(C)	Dzhogdzho	Baked contact rocks to 11–07(S)	0.333	70.4964	104.5335	5/11	246.9	–31.9	44.0	11.7	–23.9	030.7	
16-00	Dzhogdzho	Dolerite sill, same as 11–07 and perhaps 14–00	0.333	70.5117	104.5292	6/15	251.1	–32.1	66.2	7.5	–22.7	026.5	
17-00	Dzhogdzho	Dolerite dyke (mapped as P–Tr), trending 030°	1	70.5153	104.5022	12/15	228.9	–28.5	40.0	6.9	–27.3	049.6	
20-00	Lower Kotuykan	Dolerite	0(few)	70.5761	104.2278	(2 + 1c)/11	223.5	–35.6	40.7	23.0	–33.0	053.6	
12-07	Lower Kotuykan	Dolerite sill	1	70.5626	104.0303	7/15	219.9	–06.8	112.1	5.7	–18.1	061.7	
13-07	Lower Kotuykan	5 m thick dolerite sill intruding Ust-Mastakh dolostone	1	70.5634	103.8909	16/25	212.6	18.4	22.9	7.9	–07.0	071.5	
6-01	Lower Kotuykan	~10 m thick dolerite sill intruding Ust-Mastakh dolostone	1	70.53	103.91	9/20	224.2	–19.2	40.5	8.2	–23.4	055.5	
7-01	Lower Kotuykan	5–10 m thick dolerite sill intruding Ust-Mastakh dolostone	0(scatter)	70.53	103.91	0/15	Unstable	–	–	–	–	–	
8-01	Lower Kotuykan	Dolerite sill at base of high cliff	1	70.52	103.88	9/15	213.6	–15.6	18.5	12.3	–23.9	067.0	
14-07	Lower Kotuykan	Dolerite sill, 40 m above river level	1	70.5194	103.8554	10/11	214.5	–15.6	68.0	5.9	–23.7	066.1	Geochemistry group I
16-07	Kotuy	Large, continuous dolerite sill	0.1	70.3088	103.5395	8/8	212.2	–24.9	129.1	4.9	–29.4	067.0	
17-07	Kotuy	Large, continuous dolerite sill	0.1	70.3115	103.5385	4/8	219.0	–22.1	130.1	8.1	–26.4	060.0	
18-07	Kotuy	Large, continuous dolerite sill	0.1	70.3149	103.5373	6/8	208.3	–21.4	27.4	13	–28.2	071.7	

19-07	Kotuy	Large, continuous dolerite sill	0.1	70.3170	103.5392	7/8	203.6	-26.0	40.2	9.6	-31.5	076.4
20-07	Kotuy	Large, continuous dolerite sill	0.1	70.3214	103.5416	5/8	213.9	-23.5	65.4	9.5	-28.2	065.3
21-07	Kotuy	Large, continuous dolerite sill	0.1	70.3238	103.5424	6/8	206.2	-26.0	72.2	7.9	-31.1	073.5
22-07	Kotuy	Large, continuous dolerite sill	0.1	70.3271	103.5430	4/11	217.4	-23.5	55.8	12.4	-27.5	061.6
23-07	Kotuy	Large, continuous dolerite sill	0.1	70.3311	103.5411	(5 + 1c)/8	197.2	-22.5	19.3	15.9	-30.4	083.9
24-07	Kotuy	Large, continuous dolerite sill	0.1	70.3378	103.5369	5/8	216.5	-22.4	59.7	10	-27.1	062.7
25-07	Kotuy	Large, continuous dolerite sill	0.1	70.3443	103.5363	7/8	205.1	-18.4	40.0	9.7	-27.1	075.5
26-07	Kotuy	Dolerite sill	1	70.3926	103.4287	8/15	206.6	-26.0	73.8	6.5	-31.0	072.9
27-07	Kotuy	15 m wide alkaline dyke, trending 060°	1	70.4261	103.4277	5/15	201.8	-21.9	38.3	12.5	-29.4	078.7
Mean						21 sites	218.7	-20.0	30.7	5.8	-25.3	061.4
											K = 48.6	A95 = 4.6

Notes: In site abbreviations, (D) = dyke, (S) = sill, (C) = exocontact, (H) = distant host; for zero weights, (aniso = anisotropic), (few) = $n < 5$, (PLP) = present local field, (scat) = $a95 > 18^\circ$; n/N = number of samples in mean direction/number analyzed (c = great circles); GDec, GInc = mean ChRM in geographic coordinates (degrees); k , $a95$ = Fisher's (1953) precision parameter, radius($^\circ$) of the 95% cone of confidence about the mean direction; Plat, Plong = Virtual geomagnetic pole latitude, longitude ($^\circ$ = polarity inverted); Geochemistry groups and U–Pb baddeleyite ages are from Ernst et al. (2016b).

* Plat, Plong listed as antipole of the mean direction given in the table.

from antipolarity is due to a declination offset, which may be tempting to interpret as due to vertical-axis rotation between the west Anabar and Fomich areas, but continuity of exposure and near-horizontality of strata in both regions argue against such an interpretation. In addition, the lone Group 4 direction (SW-up) from Fomich has similar declination to the remainder of Group 4 directions from west Anabar. An alternative explanation for the negative reversal test is a significant age difference between the two polarities of remanence, with Siberian plate motion during the intervening time interval. Two U–Pb dated sills with the Group 4 remanence in west Anabar have ages of 1503 ± 2 and 1502 ± 2 Ma, whereas the Group 3 sill in Fomich area has a U–Pb age of 1483 ± 17 Ma (Ernst et al., 2016b). Following this interpretation, we treat the Group 3 and 4 directions as distinct from each other in our analysis.

5. Baked-contact tests

We performed several baked-contact tests (BCTs), to the extent allowable by available outcrops along the rivers.

- (1) Fomich River, site 3-04. A 50 m-wide dyke, and Burdur Formation sedimentary rocks in the exocontact, both give NE-shallow up Group 3 directions. Burdur host rocks at this site are magnetically unstable. However, site 4-04, only six km away, has the “younger sedimentary” Labaztakh direction. This is not a complete BCT, though it is suggestive of primary remanences. The baked sediment direction matches precisely the dyke direction, not the Group 3 mean, suggestive of instantaneous baking of the host rocks rather than recording a regional magnetic overprint.
- (2) Fomich River, site 24-04. A 30 m-wide dolerite dyke has a direction that is clearly within Group 3, but has scatter slightly larger than our cutoff filter ($a95 > 18^\circ$). Contact rocks were altered and thus were not sampled, but fresh Kotuykan Formation limestone 100–350 m away yielded a stable “younger sedimentary” direction. Although not a complete baked-contact test, the data suggest lack of pervasive remagnetization in the region.
- (3) Fomich River, site 25-04. A 10 m-wide dyke carries the SW-shallow, Group 4 direction (determined by 4 least-squares lines plus 2 planes), but Kotuykan Formation green and red variegated limestone strata 40 m and 150 m away bear the S-down younger sedimentary direction. The dyke's exocontact rocks are green limestone yielding an anomalous WSW-shallow direction. Although this direction is closer to the dyke remanence than that of the distant host rocks, the aggregate data are only suggestive of a positive BCT.
- (4) Upper Kotuykan River, site O-08. A subvertical dyke with exposed (i.e., minimum) width of 25 m intrudes Mukun Group sediments that were sampled at distances of 5 m, 10 m, and 20 m from the contact; all subsites share a Permian–Triassic Group 1 direction. No distant host rock was sampled, so the test is incomplete.
- (5) Upper Kotuykan River, site 181-08. A ~15 m-wide dyke and its exocontact have the same SW-shallow Group 4 direction. Distant host rocks were sampled about 500 m away, but their response to thermal demagnetization was chaotic; so the test is incomplete.
- (6) Ilya River, site 37-07. A 12 m-wide dyke plus exocontact, plus distant Burdur Fm host rock, all give the SW-up Group 4 direction. The “distant” host rock samples were collected at 2 m and 10 m away from the contact, so the zone of directional concordance only slightly exceeds the canonical half-dyke-width rule for contact remagnetization. The presence

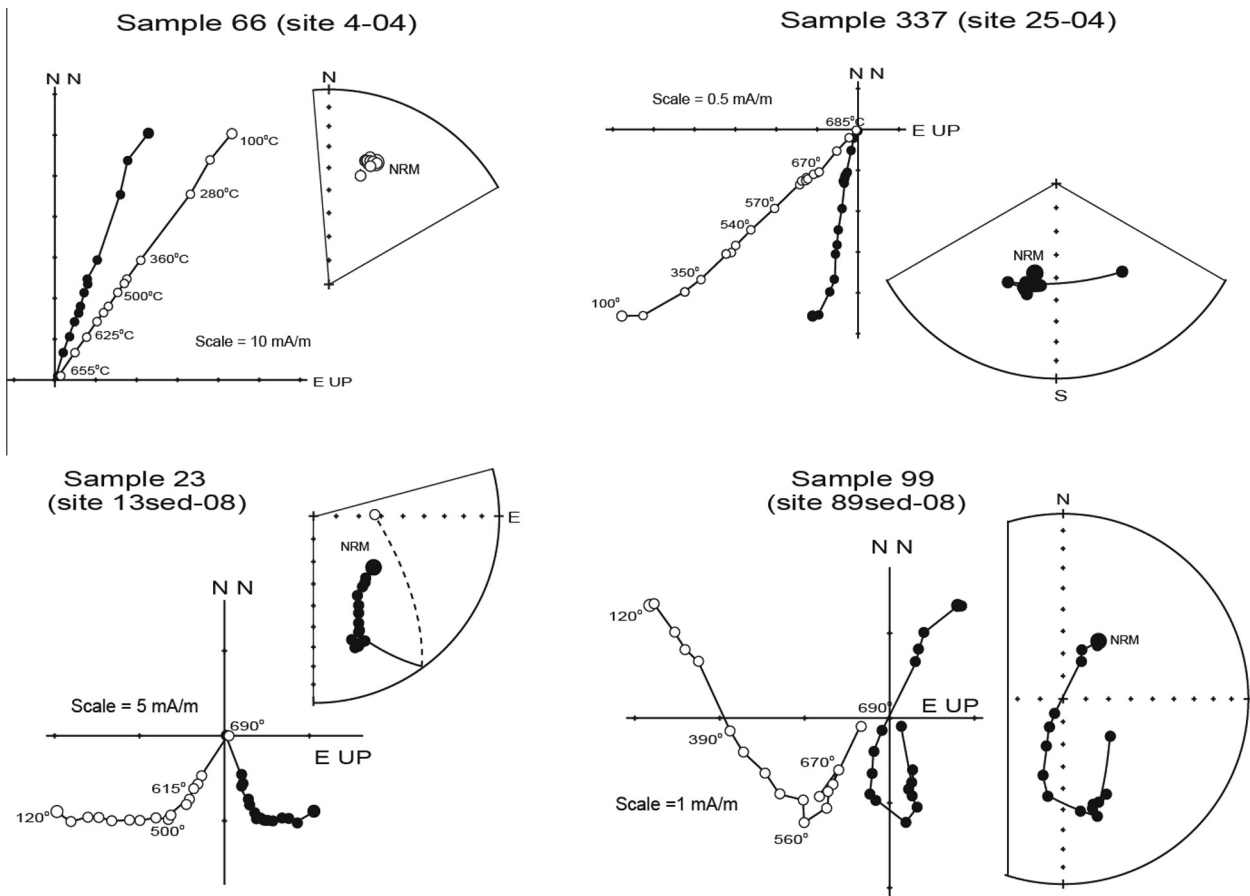


Fig. 3. Orthogonal demagnetization diagrams and equal-angle stereonet plots of sedimentary samples from sites distant to mapped intrusions. Upper row: younger sedimentary succession from Fomich River valley, Labastakh Formation (left) and Kotuykan Formation (right). Lower row: older sedimentary succession from the Western Anabar region, Ust-II'ya Formation (left) and Burdur Formation (right). In all orthogonal demagnetization plots, closed symbols lie within the horizontal projection and open symbols lie within the vertical projection. NRM = natural remanent magnetization. All temperatures are in °C.

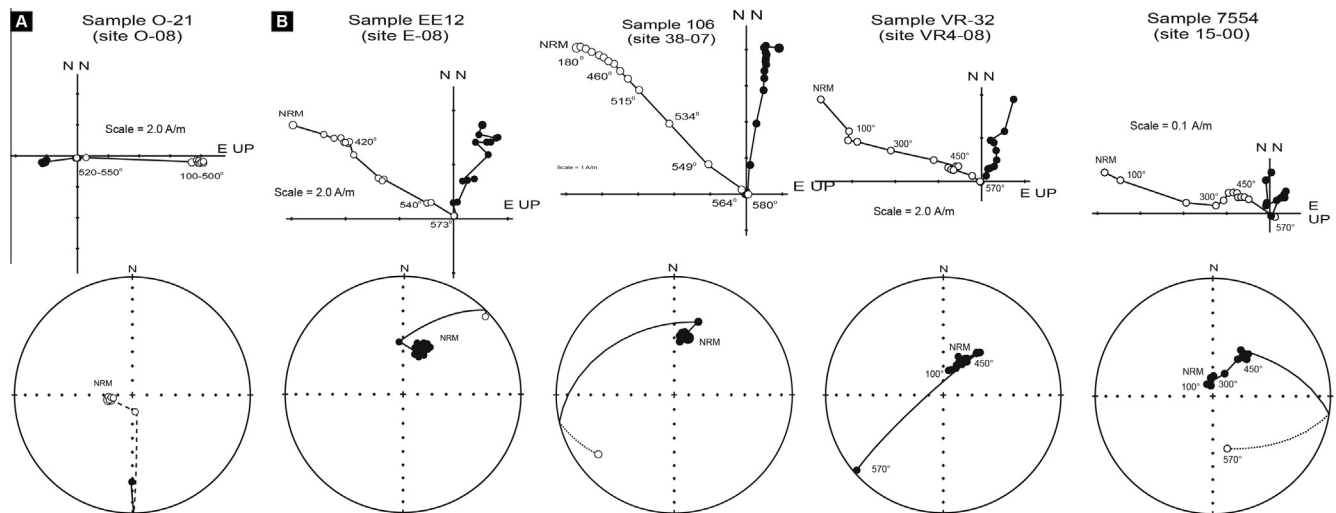


Fig. 4. Representative orthogonal demagnetization diagrams and equal-area stereonet plots of (A) sites inferred to be of Permian-Triassic age based on steep west-up or east-down Group 1 remanence direction, and (B) sites carrying the enigmatic north-down or south-up Group 2 direction. Symbols as in Fig. 3.

of a N-down Group 2 direction at site 36-07, only 1.2 km away, argues against widespread regional overprinting.

- (7) Middle Kotuykan River, site 39-07. A 20 m-wide dyke has a NE-shallow Group 3 direction shared by the distant host rock (Kotuykan Formation gray siltstone, 720 m away from the contact). The dyke's exocontact has a direction

intermediary between the Group 2 and 3 directions, but with a large a_{95} value so it is excluded from both means. The baked-contact test is considered to be inconclusive.

- (8) Dzhogdzh River, site 5-07. A 3–4 m wide mafic dyke has a steep-up Group 1 (Permian-Triassic) direction. Its exocontact has the same steep-up direction, but the distant host

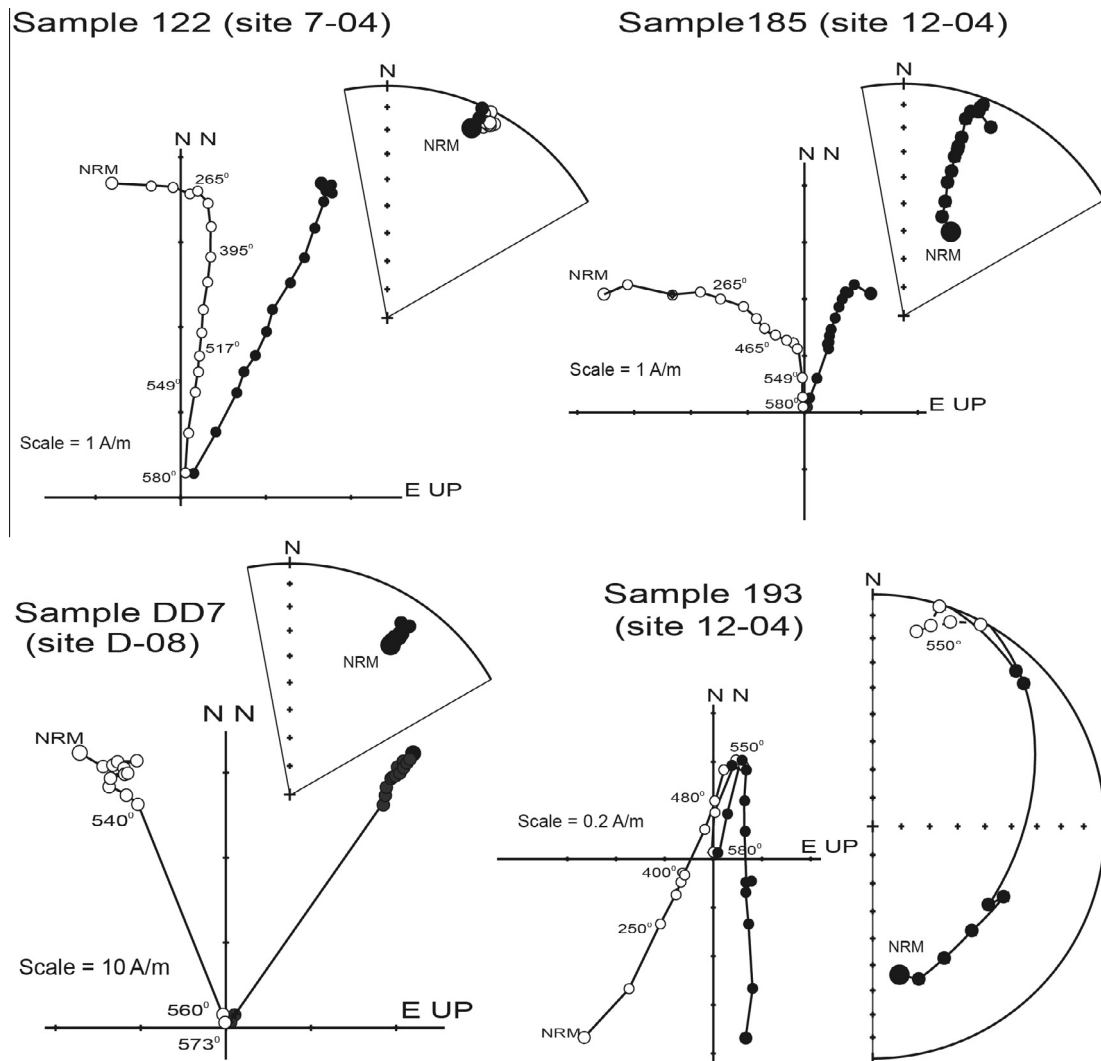


Fig. 5. Representative orthogonal demagnetization diagrams and equal-area stereonet plots of sites carrying the northeast-shallow Group 3 characteristic remanence direction. Symbols as in Fig. 3.

rock (Kotuykan red dolomite) has a N-down Group 2 direction, as does the red dolomite at the next site, ~400 m away. In addition, site 4-07 (dolerite sill) is also only ~600 m distant from the baked-contact test, and has a SW-up Group 4 ChRM. The combined results from these sites suggest that both the N-down Group 2 direction and the SW-up Group 4 direction pre-date the Permian–Triassic intrusion, which itself carries a primary Group 1 remanence.

- (9) Dzhogdzho River, site 11-07 (sill with U–Pb age of 1501.6 ± 1.9 Ma). Both intrusion and exocontact have same SW-up Group 4 direction. Mafic intrusions of various ages are pervasive in this region of the lower Dzhogdzho River, so it was not possible to find host sedimentary rocks unaffected by their influence and the test is thus incomplete.

To summarize, none of the baked-contact tests conclusively demonstrate a primary remanence for either the N-D “enigmatic” Group 2 ChRM direction or the NE/SW shallow ChRM directions of Groups 3 and 4. However, there are strong suggestions of primary remanence in Group 3 (Fomich River sites 3 and 24); and Groups 2 and 4 are both likely older than Permian–Triassic (Dzhogdzho River site 5-07)—assuming that each group contains a pure, uncontaminated representation of the local geomagnetic field at some time in the past. There remains the possibility that

any of those non-trap ChRM groups, particularly the N-down Group 2 direction, could be a mixture of other components, as discussed next.

6. Interpretation of characteristic remanence directions

Based on the information presented above, either the dominantly N-down Group 2 direction or the nearly antipodal Group 3 and 4 directions could plausibly be primary. The Group 3 and 4 data are similar to those reported from nearly coeval rocks in the Olenëk uplift in northeastern Siberia (Wingate et al., 2009) and to some directions obtained from dykes of the eastern Anabar uplift (Ernst et al., 2000). Among all groups, multiply sampled intrusions yield site-mean directions that are well clustered relative to the entire spread of data, implying a positive “secular variation test” as one would expect from sampling thermal-remanent magnetizations (TRMs) from quickly cooled intrusions (Halls, 1986). Groups 2–4 are distributed throughout large areas of our sampling region, although Group 2 is restricted to the west Anabar subregion (upper Kotuykan to Dzhogdzho Rivers). Within Groups 3 and 4, a rough correlation with stratigraphy may be evident, with Group 3 among the lower levels of sill intrusion, and Group 4 among the higher levels (Figs. 1 and 2).

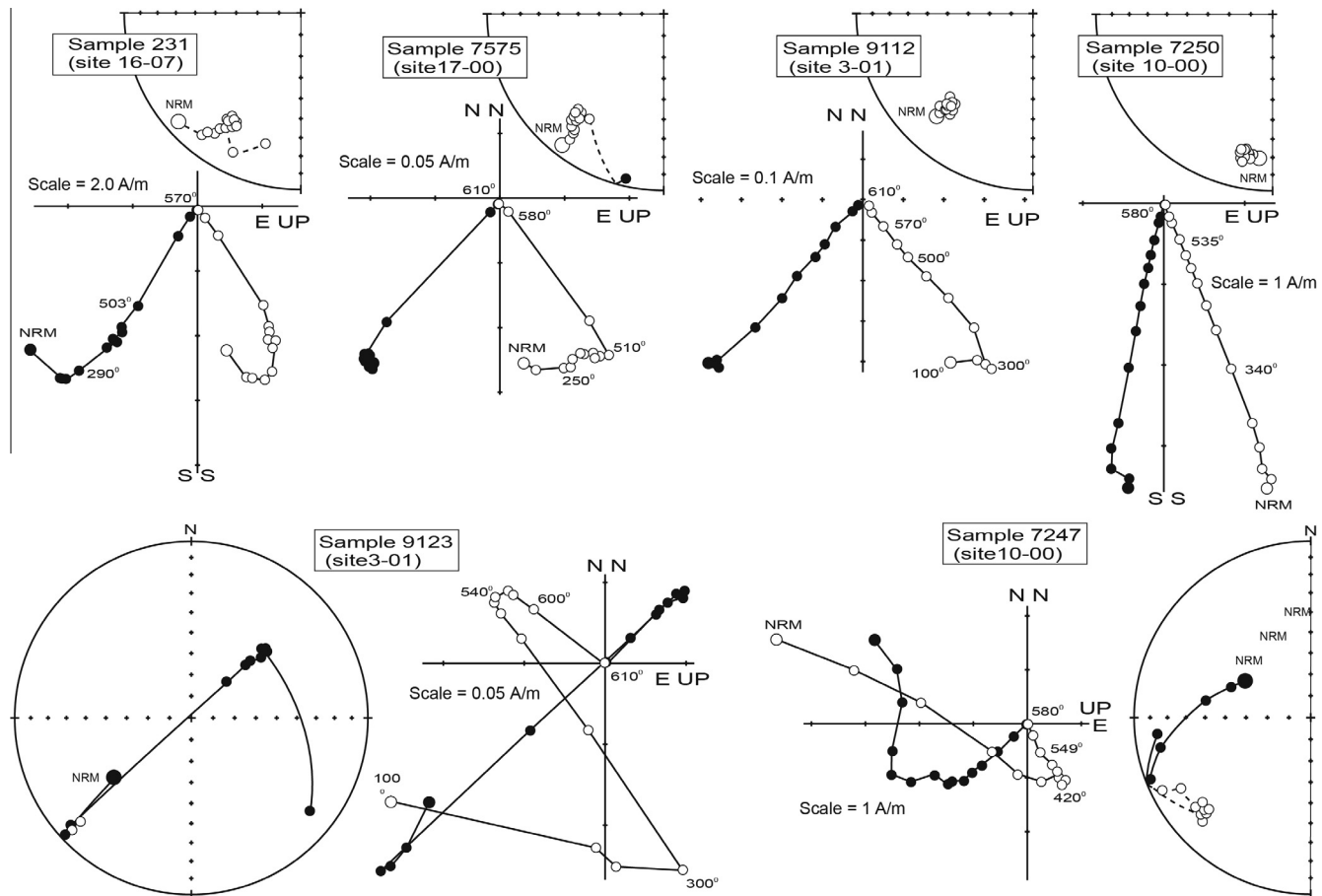


Fig. 6. Representative orthogonal demagnetization diagrams and equal-area stereonet plots of sites carrying the southwest-shallow Group 4 characteristic remanence direction. Symbols as in Fig. 3.

The first class of explanations for the difference between the N-down “enigmatic” Group 2 component and the NE/SW shallow Groups 3 and 4 components assumes that they all accurately record the local geomagnetic field at the time of remanence acquisition, recording excursions of either Siberian APW or the mid-Proterozoic geodynamo. We suspect an APW explanation is unlikely, because Group 2 is identified in the Upper Kotuykan River sill site VR1-5 (1493 ± 9 Ma) whereas Group 4 is found in sills of the same age, within error: Dzhogdzhoh River site 11-07 (1502 ± 2 Ma) and Kotuy River sites 16-07 to 25-07 (1503 ± 2 Ma). Stretching the age uncertainties to their limits, one would require 49° of APW in a span of only 21 million years, corresponding to a minimum 26 cm/yr rate of continental motion. A slight age difference between directional groups could perhaps in principle be detectable by subtle geochemical variations, and indeed there are two distinct trace-element geochemical groups of intrusions described by Ernst et al. (2016b); however, those two groups do not correspond to the paleomagnetic directional groups (Table 1). If the paleomagnetic discrepancy is to be explained by a geomagnetic excursion, then the enigmatic Group 2 more likely records the anomalous field because it is less abundant across the field area. Nonetheless, it then becomes puzzling why the excursion would be observed in so many rocks spread across ~ 3000 km², including not only mafic intrusions but also redbeds, the latter presumably bearing a thermochemical remanence unlikely to be acquired at precisely the same time. Most troubling for this class of explanation, however, is the fact that both Group 2 and Group 4 directions are found at different sites within the same intrusion, for example

Dzhogdzhoh sites 15-00 (Gr. 2), 11-07 (Gr. 4) and 16-00 (Gr. 4). A similar discrepancy exists at Dzhogdzhoh sites 1-07 (Gr. 4) and 2-07 (Gr. 2), both from the same intrusion, although the 2-07 ChRM is the only southerly-upward polarization of the Group 2 set—one could choose to consider it as a marginal member of Group 4, but then the discrepancy between it and 1-07 from the same intrusion remains a challenge for APW or geomagnetic explanations of all the directional discordances in our dataset.

A second class of explanations for the Group 2–4 directional discordance invokes rock-magnetic artifacts of either anisotropy or component mixing. Anisotropic effects are unlikely because none of the sampled rocks are visibly anisotropic as would be necessary to account for the $\sim 30^\circ$ directional discordance. The Group 2 direction, being N-down directed at Northern Hemisphere sites, is inherently suspect as being contaminated by a viscous remanent magnetization (VRM) acquired in the present Earth field, perhaps partially overprinting Group 3 northeasterly ChRMs. This seems unlikely, however, because (a) Group 2 samples exhibited straight-line demagnetization trajectories that would require coincidentally identical unblocking spectra between the two components, (b) Group 2 sites were typically Fisher-distributed, with no preferred elongation direction at either the within-site or between-site hierarchical level, (c) Site 15-00 has a Group 2 direction but the adjacent sites 14-00 and 16-00 (the former possibly and the latter definitely from the same intrusion) have SW-seeking ChRM directions (Group 4) rather than NE-seeking Group 3 directions, and (d) Group 2 directions in red dolomite (sites 5-07 and 6-07) and red sandstones (site 105sed-08) render

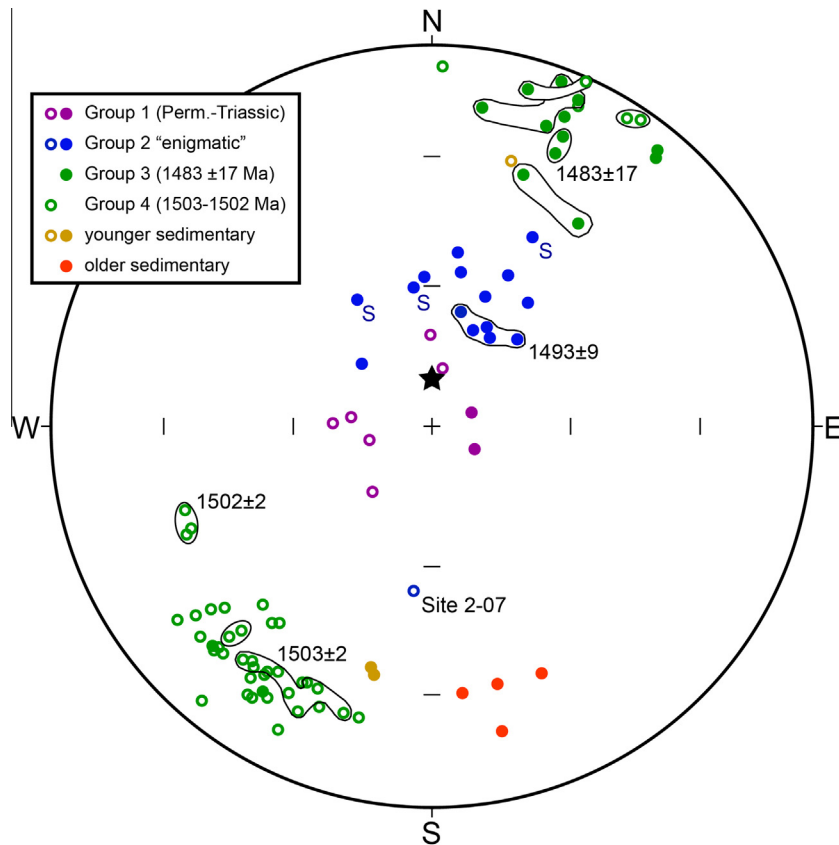


Fig. 7. Equal-area stereographic projection of all site means reported in this study, color coded by remanence grouping as in Table 1 (color-coded as in Fig. 1). Solid symbols are in the lower hemisphere; open symbols are in the upper hemisphere. Each irregular envelope surrounds multiple sites collected from the same intrusion. U–Pb baddeleyite ages are in Ma (Ernst et al., 2016b). Site 2-07 is discussed in text. S = sedimentary site within Group 2. Star is the present dipole field direction for the sampling area.

a VRM interpretation unlikely because those redbed sites are unlikely to contain multi-domain magnetite, the typical carrier of VRMs.

The enigmatic Group 2 direction could alternatively be interpreted as a contaminated partial overprint from Permian–Triassic traps. It is noted that 8 out of 11 of the Group 2 sites are located within 7 km of a site bearing a Permian–Triassic Group 1 direction. However, the polarity of nearest Group 1 site does not always match that of the proximal Group 2 site. Also, it seems improbable that all five sites in the single sill at the base of the succession along the upper Kotuykan River (VR1–5, dated by U–Pb on baddeleyite at 1493 ± 9 Ma) would be partially remagnetized by a trap intrusion where none is recognized in that area.

Although most samples yielded single-component behavior, some examples were observed of Group 2 partial overprinting on either a sedimentary ChRM (Fig. 3, sample 99), or one the Group 3 or Group 4 characteristic remanences (Fig. 5, sample 185; Fig. 6, sample 7247). There were only rare instances of a Group 3 or Group 4 component unblocking at lower temperatures than a Group 2 component (Fig. 6, sample 7247).

Petrographic and rock-magnetic results (Fig. 8) may shed some additional light on the origin of Group 2 remanence, although the data are far from definitive. Group 2 samples tend to be finer-grained than those of Groups 3 and 4, with pyroxene and glassy matter completely overprinted by epidote and chlorite, and creation of fine-grained opaque minerals on the chloritized pyroxene. Groups 3 and 4 tend to be coarser-grained, with ophitic and poikilo-ophitic textures. Partial to complete saussuritization affects plagioclase, and pyroxene is variably altered along grain

boundaries to amphibole, chlorite, and epidote. On the whole, samples from Groups 3 and 4 tend to be less altered than samples from Group 2.

In backscattered scanning electron microprobe (SEM) imagery, Groups 3 and 4 show variability of Fe-oxide phases, both in grain size and in morphology. Group 2 samples tend to have larger amalgamations of Fe-oxide-bearing grains with oxy-exsolution features. Group 1 Fe-oxide grains are smaller and lack distinctive internal structure. In all samples, the presence of high-temperature oxidation and solid solution decay is supported by SEM observations and microprobe analyses, and these can be considered as evidence for a primary magmatic origin of the most of magnetic minerals. Groups 3 and 4 show sufficient variability of magnetic mineralogy to corroborate the idea that recording of the ambient geomagnetic field occurred over enough time to average paleosecular variation.

Hysteresis parameters of studied samples, summarized on the plotting convention of Day et al. (1977), show that they contain single-domain and pseudo-single-domain (SD/PSD) magnetic particles, and can be considered as stable magnetic carriers over geological timescales (Fig. 8A). The Group 3 and 4 samples exhibit the greatest variability in hysteresis parameters, whereas Groups 1 and 2 are confined to the central part of the PSD field. This may indicate support for briefly emplaced and relatively homogeneous magnetic mineralogy for each of those two directional groups (Permian–Triassic and the enigmatic group). Thermomagnetic curves of bulk susceptibility versus temperature (Fig. 8B) all indicate dominant presence of near-stoichiometric magnetite, with Hopkinson peaks at temperatures immediately below 580 °C.

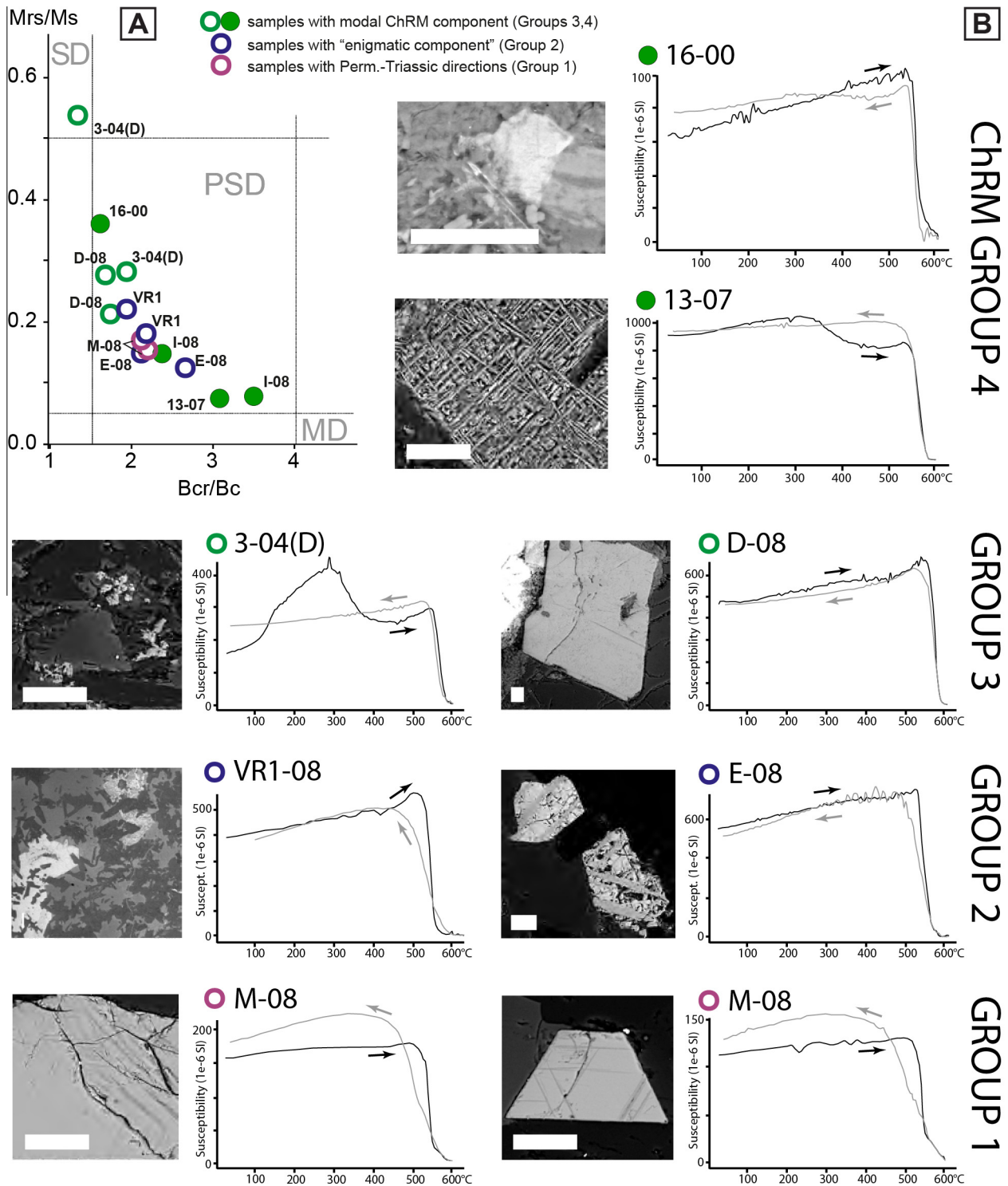


Fig. 8. Rock-magnetic data from representative samples of the four directional groups, color-coded as in Fig. 1. (A) Plot of hysteresis parameters (Mrs/Ms = ratio of saturation remanence to saturation magnetization; Bcr/Bc = ratio of coercivity of remanence to coercivity) from samples plotted against the canonical fields (Day et al., 1977) of single-domain (SD), pseudo-single-domain (PSD) and multi-domain (MD) magnetite. (B) Selected samples from each of the four characteristic remanence (ChRM) directional groups, showing SEM backscattered imagery (scale bar = 20 μ m wide for all images; the bar for VR1-08 is almost too narrow to see, as the field of view is \sim 3 mm wide), and bulk susceptibility versus temperature for heating and cooling.

These curves show more variable behavior for Groups 3 and 4, with some curves largely reversible and others irreversible. Group 2 samples are dominated by nearly reversible thermomagnetic behavior, whereas Group 1 shows consistently irreversible behavior.

Altogether, we favor the Group 3 and Group 4 magnetizations as most likely to represent primary magnetizations among the

ca. 1500 Ma intrusions around the Anabar Shield. This interpretation is mainly due to (a) greater abundance relative to the enigmatic Group 2 component, (b) various possible explanations for the Group 2 component including modest degrees of remagnetization or acquisition during geomagnetic excursions, and (c) an overall smooth progression of paleomagnetic poles through the

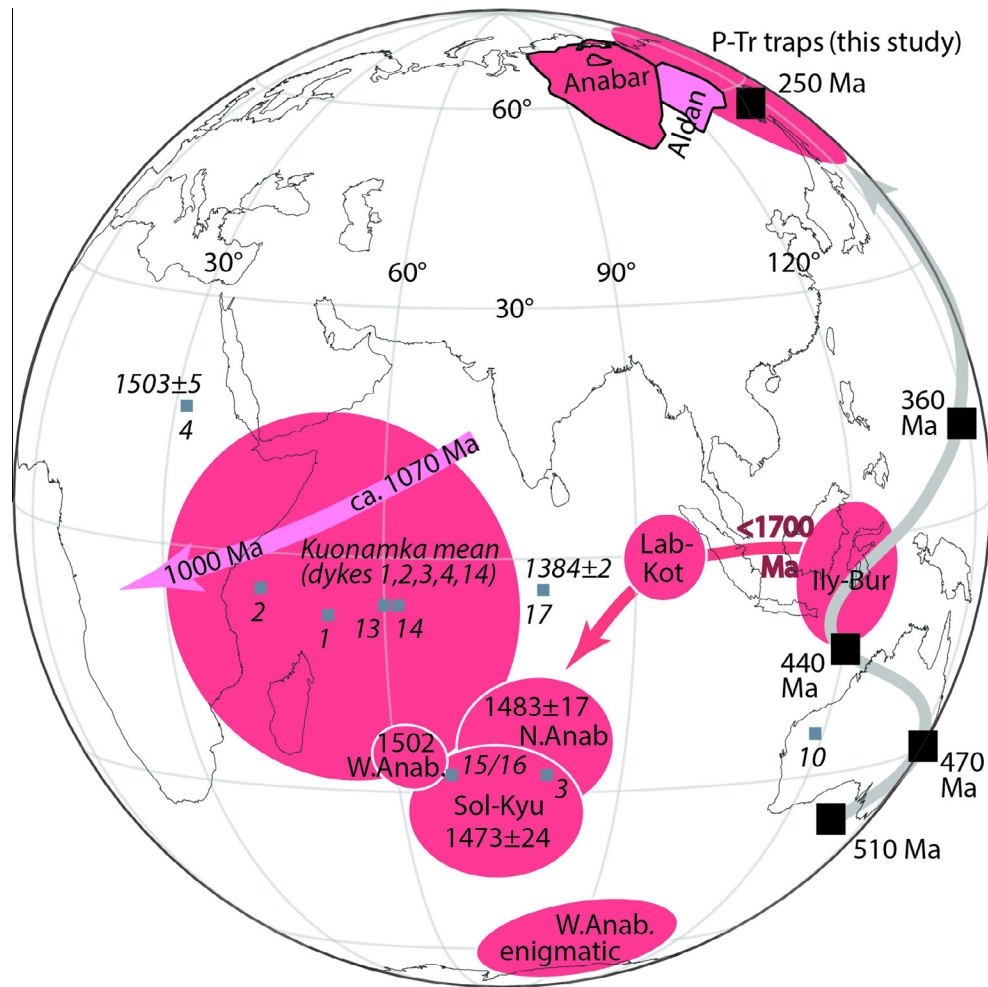


Fig. 9. New paleomagnetic poles generated in this study, compared to selected published results. Pole abbreviations follow Table 2, plus P–Tr (Permian–Triassic). Aldan block and its generalized ca. 1070–1000 Ma pole path (pink) have been restored to the Anabar reference frame in pre-Devonian time (Pavlov et al., 2008; Euler parameters from Evans, 2009). The individual site-mean virtual geomagnetic poles from Ernst et al. (2000) have italicized numeric labels and U–Pb ages. Dark squares are selected Paleozoic running-mean Siberian (Anabar frame) poles from Cocks and Torsvik (2007).

stratigraphic succession, from the older Riphean sedimentary units, to the younger sedimentary units, and finally to the Group 3 and 4 results (Fig. 9).

In addition to these arguments in favor of the Group 3 and 4 data representing the Siberian craton at ca. 1500 Ma, we note the consistency of the Group 3 and 4 poles with that of the nearly coeval Sololi-Kyutingde pole from the Olenëk area to the east (Wingate et al., 2009; Fig. 9). Our new data are similar to some results from eastern Anabar dykes (Ernst et al., 2000; Fig. 9), but our poles differ from the Kuonamka mean pole of the same study, which was assigned an age of 1503 ± 5 Ma based on U–Pb dating of one of the dykes. Fig. 9 shows how the five-dyke Kuonamka mean lies between the dated dyke's VGP and both the Olenëk pole and our new results. We follow Evans and Mitchell (2011) in interpreting the dated Kuonamka dyke's anomalous remanence—relative to the vastly more abundant Olenëk dataset of Wingate et al. (2009) and now also our northern and western Anabar results—as representing either a geomagnetic excursion or, perhaps, hitherto unrecognized (and if so, dramatic) rotations of Siberia at ca. 1500 Ma.

7. Tectonic reconstruction

As noted above, the primary goal of this study is to determine whether new paleomagnetic data from Siberia can elucidate its

position relative to Laurentia during mid-Proterozoic time. Our new Group 3 and Group 4 poles, dated at 1483 ± 17 and 1503 ± 2 Ma, respectively, can be compared to mid-Proterozoic poles from Laurentia (Table 2), in particular the St. Francois Mountains igneous province result from Meert and Stuckey (2002). Our new poles conform to earlier suggestions of a juxtaposition between the southern Siberian and northern Laurentian margins (Fig. 10). Our new poles are substantially discordant to the St. Francois Mountains pole in the Siberia-Laurentia reconstruction models of Sears and Price (1978, 2000, 2003).

The question of whether the Siberia-Laurentia fit was loose (Pisarevsky and Natapov, 2003; Pisarevsky et al., 2008) or tight (Pavlov et al., 2002; Metelkin et al., 2007; Evans and Mitchell, 2011) during mid-Proterozoic time is not addressed directly by our new poles, because they fall atop the coeval Laurentian poles about equally well in either of the two reconstructions (compare Fig. 10a and b). Other Proterozoic poles from Siberia may aid in answering this question, however. Fig. 10 shows Siberian and Laurentian poles from the interval 1750–700 Ma (Table 2). Either reconstruction accommodates the poles in a single APW path with reasonable consistency, but the most important difference occurs in the 1100–1000 Ma datasets. In a loose-fitting reconstruction (Fig. 10a), the Linok and Uchur-Maya poles (Malgina to Kandyk) fall along the 1090–1000 Ma portion of the Laurentian APW path; whereas in the tight-fitting reconstruction (Fig. 10b), the same

Table 2
Paleomagnetic poles shown in Figs. 9 and 10.

Craton/rock unit	Code	Age (Ma)	Pole(°N,°E)	A ₉₅ (°)	1234567 Q	References
<i>Siberia (Anabar Ref. frame)</i>						
Nersa complex A	Nersa	1641 ± 8	−23, 130	12	1111110 6	Metelkin et al. (2005) and Ernst et al. (2016a)
Ilya-Burdur	Ily-Bur	1690–1500	−04, 120	9	0110100 3	This study, Khudoley et al. (2015)
Labaztakh-Kotuykan	Lab-Kot	<Ily-Bur	−00, 094	5	0110111 5	This study
West Anabar intrusions	WAnab	1503 ± 2	−25, 061	5	1111100 5	This study, Ernst et al. (2016b)
North Anabar intrusions	NAnab	1483 ± 17	−24, 075	8	1110100 4	This study, Ernst et al. (2016b)
Sololi-Kyutingde	Sol-Kyu	1473 ± 24	−34, 073	10	1111100 5	Wingate et al. (2009)
Malgina Fm	Malg	<1120	15, 070 [†]	3	0111111 6	Gallet et al. (2000) and Khudoley et al. (2015)
Linok Fm	Linok	=Malgina	15, 076	8	0111111 6	Gallet et al. (2000), age from correlation
Kartochka Fm*	Kart	ca. 1050?	19, 036	12	0111101 5	Gallet et al. (2012), age interpolated from APWP
Mil'kon Fm	Milk	ca. 1050?	−06, 039 [†]	3	0111101 5	Pavlov and Gallet (2010), age interpolated
Kandyk Fm	Kand	ca. 990	−09, 019 [†]	4	1111100 5	Pavlov et al. (2002)
Kitoi mafic sheets	Kitoi	758 ± 4	01, 022	7	1111101 6	Pisarevsky et al. (2013)
<i>Laurentia</i>						
Cleaver dykes	Cleav	1740 ± 5/-4	19, 277	6	1111101 6	Irving et al. (2004)
Melville Bugt dykes	Melv	1638–1619	03, 261 ^{††}	9	1101011 6	Halls et al. (2011)
Western Channel diabase	WCh	ca. 1592	09, 245	7	1101101 5	Irving et al. (1972) and Hamilton and Buchan (2010)
St Francois Mtns	StFr	1476 ± 16	−13, 219	6	1111101 6	Meert and Stuckey (2002)
Michikamau intr. comb.	Mich	1460 ± 5	−02, 218	5	1111011 6	Emslie et al. (1976)
Spokane Fm	Spok	1470–1445	−25, 216	5	1111101 6	Elston et al. (2002)
Snowslip Fm	Snow	1463–1436	−25, 210	4	1111111 7	Elston et al. (2002)
Purcell lava	Purc	1443 ± 7	−24, 216	5	1111101 6	Elston et al. (2002)
Abitibi dikes	Abit	1141 ± 2	49, 216	14	1111111 7	Ernst and Buchan (1993), excl. A1 Halls et al. (2008)
Logan sills	Logan	1111 ± 3	47, 218	4	1111111 7	Lulea Working Group (2009) ^{†††}
Osler R – lower 3rd	OsR1	1111–1108	41, 219	4	1110111 6	Swanson-Hysell et al. (2014a)
Mamainse Point R1a	MPR1a	1111–1105	50, 227	5	1111111 7	Swanson-Hysell et al. (2014b)
Osler R – middle 3rd	OsR2	1110–1103	43, 211	8	1111111 7	Swanson-Hysell et al. (2014a)
Osler R – upper 3rd	OsR3	1105 ± 2	43, 202	4	1111111 7	Swanson-Hysell et al. (2014a)
Mamainse Point R1b	MPR1b	1110–1100	38, 206	4	1111111 7	Swanson-Hysell et al. (2014b)
Mamainse Point N1 + R2	MPmid	1100.4 ± 0.3	36, 190	5	1111111 7	Swanson-Hysell et al. (2014b)
North Shore Volcanics N	NSVN	1102–1095	36, 182	3	1110111 6	Tauxe and Kodama (2009)
Chengwatana Volcanics	Cheng	1095 ± 2	31, 186	8	1110111 6	Kean et al. (1997) and Zartman et al. (1997)
Portage Lake Volcanics	PLV	1095 ± 3	27, 178	5	1111101 6	Hnat et al. (2006)
Mamainse Point N2	MPN2	1100–1094	31, 183	3	1111111 7	Swanson-Hysell et al. (2014b)
Cardenas basalts + intrus.	Card	1091 ± 5	32, 185	8	1110101 5	Weil et al. (2003)
Lake Shore Traps	LST	1087 ± 2	23, 186	4	1111101 6	Kulakov et al. (2013)
Nonesuch Fm	None	ca. 1065?	08, 178	6	0110100 3	Symons et al. (2013), age interpolated from APWP
Freda Fm	Freda	ca. 1055?	02, 179	4	0110100 3	Henry et al. (1977), age interpolated
Jacobsville Fm (A + B)	JacAB	ca. 1040?	−09, 183	4	0110110 4	Roy and Robertson (1978), age interpolated
Chequamegon Fm	Cheq	ca. 1035?	−12, 178	5	0110100 3	McCabe and Van der Voo (1983), age interpolated
Haliburton A	Hal-A	1015 ± 15	−33, 142	6	1110000 3	Warnock et al. (2000)
Adirondack fayalite granite	Ad-fay	ca. 990	−28, 133	7	1110010 4	Brown and McEnroe (2012)
Adirondack metam. anorth.	Ad-met	ca. 970	−25, 149	12	1110010 4	Brown and McEnroe (2012)
Adirondack microcl. gneiss	Ad-mic	ca. 960	−18, 151	10	1110010 4	Brown and McEnroe (2012)
Tsezotene sills	Tzes	780 ± 2	02, 138	5	1110111 6	Park et al. (1989)
Wyoming Gunbarrel dikes	WyGB	780 ± 3	14, 129	8	1110101 5	Lulea Working Group (2009) ^{†††}
Uinta Mtn sandstone	Uinta	ca. 750	01, 161	5	1110110 5	Weil et al. (2006)
Franklin LIP (authochth.)	Frank	ca. 720	07, 162	3	1111110 6	Denysyn et al. (2009)

Notes:

The seven quality criteria and “Q” factor are described by Van der Voo (1990).

* Unit weight given to each section (N = 2).

† Euler rotation parameters of pre-Devonian Aldan block to Anabar-Angara: 60, 115, 25 (Evans, 2009).

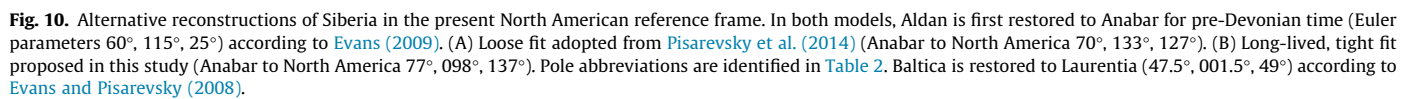
†† Euler rotation parameters of Greenland to North America: 67.5, 241.5, −13.8 (Roest and Srivastava, 1989).

††† See Pisarevsky et al. (2014).

Siberian poles correspond to slightly older Laurentian APW ages beginning closer to 1100 Ma. The youngest of these Siberian poles, Kandyk sills (Pavlov et al., 2002) is well dated at ca. 990 Ma, and accords moderately well with Grenvillian intrusive poles of about the same age from Laurentia (Warnock et al., 2000; Brown and McEnroe, 2012)—especially when considering that the paleohorizontal datums of Grenvillian intrusions are not well established—and also recognizing the caveat that internal Grenville terranes may be substantially allochthonous (Halls, 2015). The older Siberian poles from that interval, Linok and Malgina, are not precisely dated. The Malgina Formation (within the Kerpil Group) has a Pb/Pb isochron age of 1043 ± 14 Ma (Ovchinnikova et al., 2001), but it is recognized that such a value represents early diagenesis rather than deposition (Kaurova et al., 2010). Recent U–Pb detrital zircon results provide firm maximum constraints

on sedimentation, with the youngest population in basal strata of the Kerpil Group dated at 1120 ± 17 Ma (Khudoley et al., 2015). With such age constraints, both the loose-fitting and tight-fitting reconstruction options remain viable.

We are left, then, with the somewhat unsatisfactory conclusion that according to Mesoproterozoic paleomagnetic poles, both the loose-fitting and tight-fitting reconstructions of Siberia and Laurentia are possible. Each has its prediction of the ages of Kerpil Group strata, via comparison to well dated Laurentian poles. However, there is one more pole comparison that may shed additional light on this dichotomy of ideas. Recent paleomagnetic study of 758 ± 4 Ma Kitoi dykes, in SW Siberia (Pisarevsky et al., 2013), produced an excellent match with Laurentian poles in a tight-fitting reconstruction, and a rather poor match in the loose-fitting reconstruction (Fig. 10). According to the authors of that study, Siberia



If our model of billion-year tectonic stability (within the resolution of paleomagnetic data) between Siberia and northern Laurentia is correct, then all high-quality paleomagnetic poles must conform to a common APW path between the two blocks for that interval of time. As shown in Fig. 10, our model accommodates the Mesoproterozoic-Neoproterozoic poles from both cratons. Several recent paleomagnetic and geochronologic results from late Paleoproterozoic rocks, however, warrant additional discussion. In the Ulkan graben, rocks from both volcanosedimentary units and intrusive granitoids yielded paleomagnetic poles (Didenko et al., 2015). The volcanosedimentary pole from the Elgetey Formation, dated at 1732 ± 4 Ma, passes both fold and intraformational conglomerate tests, but it is highly discordant to other poles from the Siberian craton and is thus interpreted by the authors as having been deflected by local rotations during graben development. The granitoid pole, with an estimated age of 1719 Ma (Didenko et al., 2015) is more consistent with other granitoid-derived poles from southern Siberia (Didenko et al., 2009), but none of those granitoid-based data have reliable estimates of paleohorizontal. Due to this lack of structural control, neither Ulkan result can be

We thank Andrei Khudoley and an anonymous reviewer, and the handling editor Sergei Pisarevsky, for their constructive critiques of earlier versions. Volodia Pavlov and Roma Veselovskiy were partly supported by Grants RFBR ##13-05-12030 and 15-35-20599, Ministry of Education and Science of the Russian Federation Grant # 14.250.31.0017. Some of the instruments used in the

present study (JR-6 magnetometers and MFK1-A kappabridge) were purchased through the Development Program of the Lomonosov Moscow State University. Evans's contribution was supported by NSF and Yale University.

References

- Bogdanov, N.A., Khain, V.Ye., Rosen, O.M., Shipilov, V.E., Vernikovskiy, V.A., Drachev, S.S., Kostyuchenko, S.L., Kuz'michev, A.V., Sekretov, S.V., 1998. Explanatory notes for the tectonic map of the Kara and Laptev Seas and Northern Siberia. Institute of the Lithosphere of Marginal Seas, Russian Academy of Science, Moscow.
- Borradaile, G.J., Luca, K., Middleton, R.S., 2004. Low-temperature demagnetization isolates stable magnetic vector components in magnetite-bearing diabase. *Geophys. J. Int.* 157, 526–536.
- Brown, L.L., McEnroe, S.A., 2012. Paleomagnetism and magnetic mineralogy of Grenville metamorphic and igneous rocks, Adirondack Highlands, USA. *Precamb. Res.* 212–213, 57–74.
- Buchan, K.L., 2013. Key paleomagnetic poles and their use in Proterozoic continent and supercontinent reconstructions: a review. *Precamb. Res.* 238, 93–110.
- Cocks, L.R.M., Torsvik, T.H., 2007. Siberia, the wandering northern terrane, and its changing geography through the Paleozoic. *Earth Sci. Rev.* 82, 29–74.
- Condie, K.C., Rosen, O.M., 1994. Laurentia-Siberia connection revisited. *Geology* 22, 168–170.
- Day, R., Fuller, M., Schmidt, V.A., 1977. Hysteresis properties of titanomagnetites: grain size and compositional dependence. *Phys. Earth Planet. Inter.* 13, 260–266.
- Denysyn, S.W., Halls, H.C., Davis, D.W., Evans, D.A.D., 2009. Paleomagnetism and U–Pb geochronology of Franklin dykes in High Arctic Canada and Greenland: a revised age and paleomagnetic pole constraining block rotations in the Nares Strait region. *Can. J. Earth Sci.* 46, 689–705.
- Didenko, A.N., Vodovozov, V.Y., Pisarevsky, S.A., Gladkochub, D.P., Donskaya, T.V., Mazukabzov, A.M., Stanevich, A.M., Bibikova, E.V., Kirnozova, T.I., 2009. Palaeomagnetism and U–Pb dates of the Palaeoproterozoic Akitkan Group (South Siberia) and implications for pre-Neoproterozoic tectonics. In: Reddy, S. M., Mazumder, R., Evans, D.A.D., Collins, A.S. (Eds.), *Palaeoproterozoic Supercontinents and Global Evolution*, 323. Geological Society [London] Special Publication, pp. 145–163.
- Didenko, A.N., Vodovozov, V.Y., Peskov, A.Y., Guryanov, V.A., Kosynkin, A.V., 2015. Paleomagnetism of the Ulkan massif (SE Siberian platform) and the apparent polar wander path for Siberia in late Paleoproterozoic-early Mesoproterozoic times. *Precamb. Res.* 259, 58–77.
- Elston, D.P., Enkin, R.J., Baker, J., Kisilevsky, D.K., 2002. Tightening the Belt: paleomagnetic-stratigraphic constraints on deposition, correlation, and deformation of the Middle Proterozoic (ca. 1.4 Ga) Belt-Purcell Supergroup, United States and Canada. *Geol. Soc. Am. Bull.* 114, 619–638.
- Emslie, R.F., Irving, E., Park, J.K., 1976. Further paleomagnetic results from the Michikamau Intrusion, Labrador. *Can. J. Earth Sci.* 13, 1052–1057.
- Enkin, R.J., 1994. A Computer Program Package for Analysis and Presentation of Paleomagnetic Data. Pacific Geoscience Centre, Geological Survey of Canada, Victoria, p. 16p.
- Ernst, R.E., Buchan, K.L., 1993. Paleomagnetism of the Abitibi dyke swarm, southern Superior Province, and implications for the Logan Loop. *Can. J. Earth Sci.* 30, 1886–1897.
- Ernst, R.E., Buchan, K.L., Hamilton, M.A., Okrugin, A.V., Tomshin, M.D., 2000. Integrated paleomagnetism and U–Pb geochronology of mafic dikes of the eastern Anabar Shield region, Siberia: Implications for Mesoproterozoic paleolatitude of Siberia and comparison with Laurentia. *J. Geol.* 108, 381–401 <http://dx.doi.org/10.1086/314413>.
- Ernst, R.E., Hamilton, M.A., Söderlund, U., Hanes, J.A., Gladkochub, D.P., Okrugin, A. V., Kolotilina, T., Mekhonoshin, A.S., Bleeker, W., LeCheminant, A.N., Buchan, K. L., Chamberlain, K.R., Didenko, A.N., 2016a. Southern Siberia and northern Laurentia: neighbours for a quarter of Earth's history. *Nat. Geosci.* (in review).
- Ernst, R.E., Okrugin, A.V., Veselovskiy, R.V., Kamo, S.L., Hamilton, M.A., Pavlov, V., Söderlund, U., Chamberlain, K.R., Rogers, C., 2016b. The 1501 Ma Kuonamka large igneous province of northern Siberia: U–Pb geochronology, geochemistry, and links with coeval magmatism on other crustal blocks. *Russ. Geol. Geophys.* 57, 653–671.
- Evans, D.A.D., 2009. The palaeomagnetically viable, long-lived and all-inclusive Rodinia supercontinent reconstruction. In: Murphy, J.B., Keppie, J.D., Hynes, A. (Eds.), *Ancient Orogens and Modern Analogues*, 327. Geological Society of London Special Publication, pp. 371–404.
- Evans, D.A.D., 2013. Reconstructing pre-Pangean supercontinents. *Geol. Soc. Am. Bull.* 125, 1735–1751.
- Evans, D.A.D., Mitchell, R.N., 2011. Assembly and breakup of the core of Paleoproterozoic-Mesoproterozoic supercontinent Nuna. *Geology* 39, 443–446.
- Evans, D.A.D., Pisarevsky, S.A., 2008. Plate tectonics on early Earth? Weighing the paleomagnetic evidence. In: *When Did Plate Tectonics Begin on Planet Earth?*, 440 Geological Society of America Special Paper, pp. 249–263.
- Fisher, R.A., 1953. Dispersion on a sphere. *Proc. R. Soc. Lond. Ser. A* 217, 295–305.
- Frost, B.R., Avchenko, O.V., Chamberlain, K.R., Frost, C.D., 1998. Evidence for extensive Proterozoic remobilization of the Aldan Shield and implications for Proterozoic plate tectonic reconstructions of Siberia and Laurentia. *Precamb. Res.* 89, 1–23.
- Gallet, Y., Pavlov, V.E., Semikhatov, M.A., Petrov, P.Yu., 2000. Late Mesoproterozoic magnetostatigraphic results from Siberia: paleogeographic implications and magnetic field behavior. *J. Geophys. Res.* 105 (B7), 16481–16499.
- Gallet, Y., Pavlov, V.E., Halverson, G., Hulot, G., 2012. Toward constraining the long-term reversing behavior of the geodynamo: a new “Maya” superchron ~1 billion years ago from the magnetostratigraphy of the Kartochka Formation (southwestern Siberia). *Earth Planet. Sci. Lett.* 339–340, 117–126.
- Gapeev, A.K., Gribov, S.K., 2008. Magnetic properties of intrusive traps of the Siberian platform: evidence for a self-reversal of the natural remanent magnetization. *Izvestiya Phys. Solid Earth* 44, 822–838.
- Gladkochub, D.P., Wingate, M.T.D., Pisarevsky, S.A., Donskaya, T.V., Mazukabzov, A. M., Ponomarchuk, V.A., Stanevich, A.M., 2006. Mafic intrusions in southwestern Siberia and implications for a Neoproterozoic connection with Laurentia. *Precamb. Res.* 147, 260–278.
- Gladkochub, D.P., Pisarevsky, S.A., Donskaya, T.V., Ernst, R.E., Wingate, M.T.D., Söderlund, U., Mazukabzov, A.M., Sklyarov, E.V., Hamilton, M.A., Hanes, J.A., 2010a. Proterozoic mafic magmatism in Siberian craton: An overview and implications for paleocontinental reconstruction. *Precamb. Res.* 183, 660–668.
- Gladkochub, D.P., Donskaya, T.V., Wingate, M.T.D., Mazukabzov, A.M., Pisarevsky, S. A., Sklyarov, E.V., Stanevich, A.M., 2010b. A one-billion-year gap in the Precambrian history of the southern Siberian craton and the problem of the Transproterozoic supercontinent. *Am. J. Sci.* 310, 812–825.
- Halls, H.C., 1986. Paleomagnetism, structure, and longitudinal correlation of Middle Precambrian dykes from northwestern Ontario and Minnesota. *Can. J. Earth Sci.* 23, 142–157.
- Halls, H.C., 2015. Paleomagnetic evidence for ~4000 km of crustal shortening across the 1 Ga Grenville orogen of North America. *Geology* 43, 1051–1054.
- Halls, H.C., Davis, D.W., Stott, G.M., Ernst, R.E., Hamilton, M.A., 2008. The Paleoproterozoic Marathon Large Igneous Province: new evidence for a 2.1 Ga long-lived mantle plume event along the southern margin of the North American Superior Province. *Precamb. Res.* 162, 327–353.
- Halls, H.C., Hamilton, M.A., Denysyn, S.W., 2011. The Melville Bugt dyke swarm of Greenland: a connection to the 1.5–1.6 Ga Fennoscandian rapakivi granite province? In: Srivastava, R.K. (Ed.), *Dyke Swarms: Keys for Geodynamic Interpretation*. Springer-Verlag, Berlin, pp. 509–535.
- Hamilton, M.A., Buchan, K.L., 2010. U–Pb geochronology of the Western Channel Diabase, northwestern Laurentia: implications for a large 1.59 Ga magmatic province, Laurentia's APWP and paleocontinental reconstructions of Laurentia, Baltica and Gawler craton of southern Australia. *Precamb. Res.* 183, 463–473.
- Henry, S.G., Mauk, F.J., Van der Voo, R., 1977. Paleomagnetism of the upper Keweenaw sediments: the Nonesuch Shale and Freda Sandstone. *Can. J. Earth Sci.* 14, 1128–1138.
- Hnat, J.S., van der Pluijm, B.A., Van der Voo, R., 2006. Primary curvature in the Mid-Continent Rift: paleomagnetism of the Portage Lake Volcanics (northern Michigan, USA). *Tectonophysics* 425, 71–82.
- Hoffman, P.F., 1991. Did the breakout of Laurentia turn Gondwanaland inside-out? *Science* 252, 1409–1412. <http://dx.doi.org/10.1126/science.252.5011.1409>.
- Irving, E., Donaldson, J.A., Park, J.K., 1972. Paleomagnetism of the Western Channel Diabase and associated rocks, Northwest Territories. *Can. J. Earth Sci.* 9, 960–971.
- Irving, E., Baker, J., Hamilton, M., Wynne, P.J., 2004. Early Proterozoic geomagnetic field in western Laurentia: implications for paleolatitudes, local rotations and stratigraphy. *Precamb. Res.* 129, 251–270.
- Kaurova, O.K., Ovchinnikova, G.V., Gorokhov, I.M., 2010. U–Th–Pb systematics of Precambrian carbonate rocks: dating the formation and transformation of carbonate sediments. *Stratigr. Geol. Correl.* 18, 252–268.
- Kean, W.F., Williams, I., Chan, L., Feeney, J., 1997. Magnetism of the Keweenaw age Chengwatana lava flows, northwest Wisconsin. *Geophys. Res. Lett.* 24, 1523–1526.
- Kerr, J.W., 1982. Evolution of sedimentary basins in the Canadian Arctic. *Philos. Trans. R. Soc. Lond. Ser. A* 305, 193–205.
- Khudoley, A., Chamberlain, K., Ershova, V., Sears, J., Prokopyev, A., MacLean, J., Kazakova, G., Malyshev, S., Molchanov, A., Kullerud, K., Toro, J., Miller, E., Veselovskiy, R., Li, A., Chipley, D., 2015. Proterozoic supercontinental restorations: constraints from provenance studies of Mesoproterozoic to Cambrian clastic rocks, eastern Siberian Craton. *Precamb. Res.* 259, 78–94.
- Kirschvink, J.L., 1980. The least-squares line and plane and the analysis of palaeomagnetic data. *Geophys. J. R. Astronom. Soc.* 62, 699–718.
- Kráša, D., Shcherbakov, V.P., Kunzmann, T., Petersen, N., 2005. Self-reversal of remanent magnetization in basalts due to partially oxidized titanomagnetites. *Geophys. J. Int.* 162, 115–136.
- Kulakov, E.V., Smirnov, A.V., Diehl, J.F., 2013. Paleomagnetism of ~1.09 Ga Lake Shore Traps (Keweenaw Peninsula, Michigan): new results and implications. *Can. J. Earth Sci.* 50, 1085–1096.
- McCabe, C., Van der Voo, R., 1983. Paleomagnetic results from the upper Keweenaw Chequamegon Sandstone: implications for red bed diagenesis and Late Precambrian apparent polar wander of North America. *Can. J. Earth Sci.* 20, 105–112.
- McFadden, P.L., McElhinny, M.W., 1990. Classification of the reversal test in palaeomagnetism. *Geophys. J. Int.* 103, 725–729.
- Meert, J.G., Stucky, W., 2002. Revisiting the paleomagnetism of the 1.476 Ga St. Francois Mountains igneous province, Missouri. In: *Tectonics* 21 (2). <http://dx.doi.org/10.1029/2000TC001265>.

- Metelkin, D.V., Belonosov, I.V., Gladkochub, D.P., Donskaya, T.V., Mazukabzov, A.M., Stanevich, A.M., 2005. Paleomagnetic directions from Nersa intrusions of the Biryusa Terrane, Siberian Craton, as a reflection of tectonic events in the Neoproterozoic. *Russ. Geol. Geophys.* 46, 398–413.
- Metelkin, D.V., Vernikovskiy, V.A., Kazansky, A.Yu., 2007. Neoproterozoic evolution of Rodinia: constraints from new paleomagnetic data on the western margin of the Siberian craton. *Russ. Geol. Geophys.* 48, 32–45.
- Nikishin, A.M., Sobornov, K.O., Prokopiev, A.V., Frolov, S.V., 2010. Tectonic Evolution of the Siberian Platform during the Vendian and Phanerozoic. *Mosc. Univ. Geol. Bull.* 65, 1–16. <http://dx.doi.org/10.3103/S0145875210010011>.
- Ovchinnikova, G.V., Semikhatov, M.A., Vasil'eva, I.M., Gorokhov, I.M., Kaurova, O.K., Podkovyrov, V.N., Gorokhovskii, B.M., 2001. Pb–Pb age of limestones of the middle Riphean Malgina Formation, the Uchur-Maya region of east Siberia. *Stratigr. Geol. Correl.* 9, 527–539.
- Park, J.K., Norris, D.K., Laroche, A., 1989. Paleomagnetism and the origin of the Mackenzie Arc of northwestern Canada. *Can. J. Earth Sci.* 26, 2194–2203.
- Pavlov, V., Gallet, Y., 2010. Variations in geomagnetic reversal frequency during the Earth's middle age. *Geochem. Geophys. Geosyst.* 11, Q01Z10. <http://dx.doi.org/10.1029/2009GC002583>.
- Pavlov, V.E., Petrov, P.Yu., 1997. Paleomagnetism of the Riphean deposits in the Irkineeva uplift, Yenisei range: new evidence for the integrity of the Siberian platform in the middle Riphean. *Izvestiya Phys. Solid Earth* 33, 464–475.
- Pavlov, V.E., Gallet, Y., Petrov, P.Yu., Zhuravlev, D.Z., Shatsillo, A.V., 2002. Uy series and late Riphean sills of the Uchur-Maya area: isotopic and palaeomagnetic data and the problem of the Rodinia supercontinent. *Geotectonics* 36, 278–292.
- Pavlov, V., Bachtadse, V., Mikhailov, V., 2008. New Middle Cambrian and Middle Ordovician palaeomagnetic data from Siberia: Llandelian magnetostratigraphy and relative rotation between the Aldan and Anabar-Angara blocks. *Earth Planet. Sci. Lett.* 276, 229–242.
- Pavlov, V.E., Fluteau, F., Veselovskiy, R.V., Fetisova, A.M., Latyshev, A.V., 2011. Secular geomagnetic variations and volcanic pulses in the Permian-Triassic Traps of the Norilsk and Maimecha-Kotui Provinces. *Izvestiya Phys. Solid Earth* 47 (5), 402–417.
- Pisarevsky, S.A., Natapov, L.M., 2003. Siberia and Rodinia. *Tectonophysics* 375, 221–245. <http://dx.doi.org/10.1016/j.tecto.2003.06.001>.
- Pisarevsky, S.A., Natapov, L.M., Donskaya, T.V., Gladkochub, D.P., Vernikovskiy, V.A., 2008. Proterozoic Siberia: a promontory of Rodinia. *Precamb. Res.* 160, 66–76. <http://dx.doi.org/10.1016/j.precamres.2007.04.016>.
- Pisarevsky, S.A., Gladkochub, D.P., Konstantinov, K.M., Mazukabzov, A.M., Stanevich, A.M., Murphy, J.B., Tait, J.A., Donskaya, T.V., Konstantinov, I.K., 2013. Paleomagnetism of Cryogenian Kitoi mafic dykes in South Siberia: implications for Neoproterozoic paleogeography. *Precamb. Res.* 231, 372–382.
- Pisarevsky, S.A., Elming, S., Pesonen, L.J., Li, Z.-X., 2014. Mesoproterozoic paleogeography: supercontinent and beyond. *Precamb. Res.* 244, 207–225.
- Rainbird, R.H., Stern, R.A., Khudoley, A.K., Kropachev, A.P., Heaman, L.M., Sukhorukov, V.I., 1998. U–Pb geochronology of Riphean sandstone and gabbro from southeast Siberia and its bearing on the Laurentia-Siberia connection. *Earth Planet. Sci. Lett.* 164, 409–420.
- Roest, W.R., Srivastava, S.P., 1989. Seafloor spreading in the Labrador Sea: a new reconstruction. *Geology* 17, 1000–1004.
- Rosen, O.M., 2003. The Siberian craton: tectonic zonation and stages of evolution. *Geotectonics* 37, 175–192.
- Rosen, O.M., Condie, K.C., Natapov, L.M., Nozhkin, A.D., 1994. Archean and early Proterozoic evolution of the Siberian craton: a preliminary assessment. In: Condie, K.C. (Ed.), *Archean Crustal Evolution*, 11. Elsevier, Developments in Precambrian Geology, pp. 411–459.
- Roy, J.L., Robertson, W.A., 1978. Paleomagnetism of the Jacobsville Formation and the apparent polar path for the interval –1100 to –670 m.y. for North America. *J. Geophys. Res.* 83, 1289–1304.
- Sears, J.W., Price, R.A., 1978. The Siberian connection: a case for the Pre-cambrian separation of the North American and Siberian cratons. *Geology* 6, 267–270.
- Sears, J.W., Price, R.A., 2000. New look at the Siberian connection: no SWEAT. *Geology* 28, 423–426.
- Sears, J.W., Price, R.A., 2003. Tightening the Siberian connection to western Laurentia. *Geol. Soc. Am. Bull.* 115, 943–953.
- Shcherbakov, V.P., Latyshev, A.V., Tselmovich, V.A., Veselovskiy, R.V., 2015. Causes of appearance of spurious antipodal component during stepwise thermomagnetization of dolerite's NRM. In: *Proceedings of all-Russia school-seminar on problems of paleomagnetism and rockmagnetism, Moscow-Borok, 9–12 November*, pp. 258–274 (in Russian).
- Smethurst, M.A., Khramov, A.N., Torsvik, T.H., 1998. The Neoproterozoic and Palaeozoic palaeomagnetic data for the Siberian platform: from Rodinia to Pangea. *Earth Sci. Rev.* 43, 1–24.
- Swanson-Hysell, N.L., Vaughan, A.A., Mustain, M.R., Asp, K.E., 2014a. Confirmation of progressive plate motion during the Midcontinent Rift's early magmatic stage from the Osler Volcanic Group, Ontario, Canada. *Geochem. Geophys. Geosyst.* 15, 2039–2047.
- Swanson-Hysell, N.L., Burgess, S.D., Maloof, A.C., Bowring, S.A., 2014b. Magmatic activity and plate motion during the latent stage of Midcontinent Rift development. *Geology* 42, 475–478.
- Symons, D.T.A., Kawasaki, K., Diehl, J.F., 2013. Age and genesis of the White Pine stratiform copper mineralization, northern Michigan, USA, from paleomagnetism. *Geofluids* 13, 112–126.
- Tauxe, L., Kodama, K.P., 2009. Paleosecular variation models for ancient times: clues from Keweenaw lava flows. *Phys. Earth Planet. Inter.* 177, 31–45.
- Van der Voo, R., 1990. The reliability of paleomagnetic data. *Tectonophysics* 184, 1–9.
- Veselovskiy, R.V., Pavlov, V.E., Petrov, P.Yu., 2009. New paleomagnetic data on the Anabar Uplift and the Uchur-Maya region and their implications for the paleogeography and geological correlation of the Riphean of the Siberian Platform. *Izvestiya Phys. Solid Earth* 45 (7), 545–566.
- Warnock, A.C., Kodama, K.P., Zeitler, P.K., 2000. Using thermochronology and low-temperature demagnetization to accurately date Precambrian poles. *J. Geophys. Res.* 105, 19435–19453.
- Weil, A.B., Geissman, J.W., Heizler, M., Van der Voo, R., 2003. Paleomagnetism of Middle Proterozoic mafic intrusions and Upper Proterozoic (Nankoweap) red beds from the Lower Grand Canyon Supergroup, Arizona. *Tectonophysics* 375, 199–220.
- Weil, A.B., Geissman, J.W., Ashby, J.M., 2006. A new paleomagnetic pole for the Neoproterozoic Uinta Mountain supergroup, Central Rocky Mountain States, USA. *Precamb. Res.* 147, 234–259.
- Williams, S., Müller, R.D., Landgrebe, T.C.W., Whittaker, J.M., 2012. An open-source software environment for visualizing and refining plate tectonic reconstructions using high resolution geological and geophysical data sets. *GSA Today* 22 (4/5). <http://dx.doi.org/10.1130/GSATG139A.1>.
- Wingate, M.T.D., Pisarevsky, S.A., Gladkochub, D.P., Donskaya, T.V., Konstantinov, K.M., Mazukabzov, A.M., Stanevich, A.M., 2009. Geochronology and paleomagnetism of mafic igneous rocks in the Olenek Uplift, northern Siberia: Implications for Mesoproterozoic supercontinents and paleogeography. *Precamb. Res.* 170, 256–266. <http://dx.doi.org/10.1016/j.precamres.2009.01.004>.
- Zartman, R.E., Nicholson, S.W., Cannon, W.F., Morey, G.B., 1997. U–Th–Pb zircon ages of some Keweenaw Supergroup rocks from the south shore of Lake Superior. *Can. J. Earth Sci.* 34, 549–561.